land

MDPI

Article

Geospatial and Sentinel-2 Analysis of Mediterranean Wildfire Severity and Land-Cover Patterns in Greece During the 2024 Fire Season

Ignacio Castro-Melgar [1], Eleftheria Basiou [2], Ioannis Athinelis [3], Efstratios-Aimilios Katris [3], Maria Zacharopoulou [3], Ioanna-Efstathia Kalavrezou [3], Artemis Tsagkou [3] and Issaak Parcharidis [3,*]

[1] Department of Geography and Land Management, University of Zaragoza, 50009 Zaragoza, Spain; icastro@unizar.es
[2] Department of Geology and Geoenvironment, National and Kapodistrian University of Athens, 15771 Athens, Greece; eleutheriaba@geol.uoa.gr
[3] Department of Geography, Harokopio University of Athens, 17676 Athens, Greece; gp222301@hua.gr (I.A.); gp223309@hua.gr (E.-A.K.); gp223304@hua.gr (M.Z.); gs21779@hua.gr (I.-E.K.); gp223314@hua.gr (A.T.)
* Correspondence: parchar@hua.gr

Abstract

Wildfires pose increasing challenges for Mediterranean landscapes, making rapid and reliable mapping of burn severity essential for management and recovery planning. This study applies an integrated geospatial workflow to wildfires that occurred in Greece during the 2024 summer season. Sentinel-2-derived dNBR and RBR indices were used to map burn severity, while CORINE Land Cover and Tree Cover Density datasets provided complementary context for interpreting how severity varied across different vegetation types and canopy-density conditions. A one-way ANOVA was used to summarize differences in burned area among severity classes. The results show that low and moderate-low severity levels dominated most fire perimeters, whereas high-severity patches were spatially limited and typically coincided with densely forested areas. Validation against Copernicus Emergency Management Service data yielded an overall agreement of approximately 94%, indicating that the applied multispectral workflow produced severity extents broadly consistent with independent operational products. By applying a consistent methodology across multiple fire events, this study demonstrates the value of combining spectral indices with land-cover information for interpreting severity patterns and supporting post-fire management. The findings highlight the usefulness of freely accessible remote sensing data for timely fire assessment in Mediterranean environments and provide a basis for future multi-regional and multi-year comparisons.

Keywords: wildfires; Sentinel-2; Copernicus; mediterranean forests; natural hazards

Academic Editor: Martin Boltiziar

Received: 30 December 2025
Revised: 6 February 2026
Accepted: 14 February 2026
Published: 15 February 2026

1. Introduction

The Mediterranean region is a major hotspot for climate change [1]. Greece is located in the southeastern region of Europe, characterized by a Mediterranean climate, marked by mild, wet winters and hot, dry summers [2]. The region is particularly susceptible to climate change, experiencing intensified heatwaves, exacerbated droughts, and an elevated risk of coastal flooding [3]. It has experienced a rise in surface temperatures, now exceeding preindustrial levels by 1.5 °C. Global warming is strongly linked to wildfires, increasing the frequency of fire occurrences [4]. Drought conditions have become more severe and

recurrent, particularly in the northern Mediterranean region. Sea surface temperatures have risen at a rate of approximately 0.29–0.44 °C per decade since the early 1980s, with more pronounced increases observed in the eastern basin [5].

Regions with a Mediterranean climate are highly prone to wildfires due to hot, dry summers and cool, wet winters. Climate change is adversely affecting the frequency, intensity, and spread of forest fires, and this trend is expected to persist [6]. These recurrent wildfire events serve as a major driver of ecological change in the region [7]. The size and intensity of wildfires vary based on climate and fuel characteristics, leading to differing levels of tree mortality and landscape changes [8]. Also, extreme weather conditions, such as prolonged heat, drought, and strong winds, can trigger the escalation of wildfires into mega-fire events, resulting in widespread environmental degradation, threats to human life, and significant atmospheric greenhouse gas emissions [9]; overall, it can be inferred that large forest fires pose a serious environmental challenge across Mediterranean areas [10]. Forest fire risk is escalating, with the Mediterranean region being particularly affected due to increasingly unfavorable weather conditions. In addition, future increases in greenhouse gas emissions are expected to enhance wildfire susceptibility in central and northern European regions, extending even to high-altitude mountainous environments [11].

Due to the lack of fire intensity data, fire severity is used as a proxy to assess the impact on ecosystems. Fire severity highlights the extent of organic matter loss or consumption both above and below ground and is influenced by vegetation type, soil characteristics, and moisture content [12]. Wildfires have both immediate and long-term effects, including significant property damage, infrastructure destruction, ecosystem disruption, and loss of life [13]. In Greece, agricultural installations and greenhouses often suffer damage due to their location in rural interface zones, even during lower-severity fires [14]. This destruction impacts small-scale farmers with limited resources, weakening their food and economic security [15].

Remote sensing technologies play a key role in natural hazard management, offering capabilities for monitoring and assessing environmental hazards. These technologies provide insights into the detection, evaluation, and mitigation of events such as earthquakes, volcano eruptions, landslides, floods, and wildfires, enhancing disaster response and risk reduction efforts [16–21]. By leveraging remote sensing data and the Geographic Information System (GIS), fire risk maps can be created, considering factors such as vegetation, fuel loads, topography, weather conditions, and historical fire patterns [22].

Advances in satellite-based monitoring have improved the ability to map post-fire effects, yet there remains a need for integrated frameworks that combine spectral severity metrics, landscape information, and independent validation to produce rapid and comparable assessments across multiple wildfire events. This gap is particularly evident in Mediterranean regions, where heterogeneous vegetation and rugged terrain complicate the interpretation of burn patterns.

In this study, we analyze eleven wildfires that occurred in Greece during the 2024 summer season using a unified workflow that integrates Sentinel-2 multispectral data (Figure 1) as well as burn-severity indices, including the Normalized Burn Ratio (NBR) and its derivatives (differenced Normalized Burn Ratio; dNBR and Relative Burn Ratio; RBR), which are widely applied to detect burned areas and quantify burn severity. In addition, the Normalized Difference Water Index (NDWI) was used during preprocessing to exclude water bodies and improve analysis accuracy. We used the CORINE Land Cover and Tree Cover Density datasets, with a one-way analysis of variance (ANOVA) to assess the distribution of burned area across severity levels.

The one-way analysis of variance was applied to evaluate whether statistically significant differences existed among the four severity classes. Specifically, the independent

variable was burn severity level, classified into four categorical groups: Low Severity, Moderate–Low Severity, Moderate–High Severity, and High Severity. Burned area (expressed in km^2) was the dependent variable.

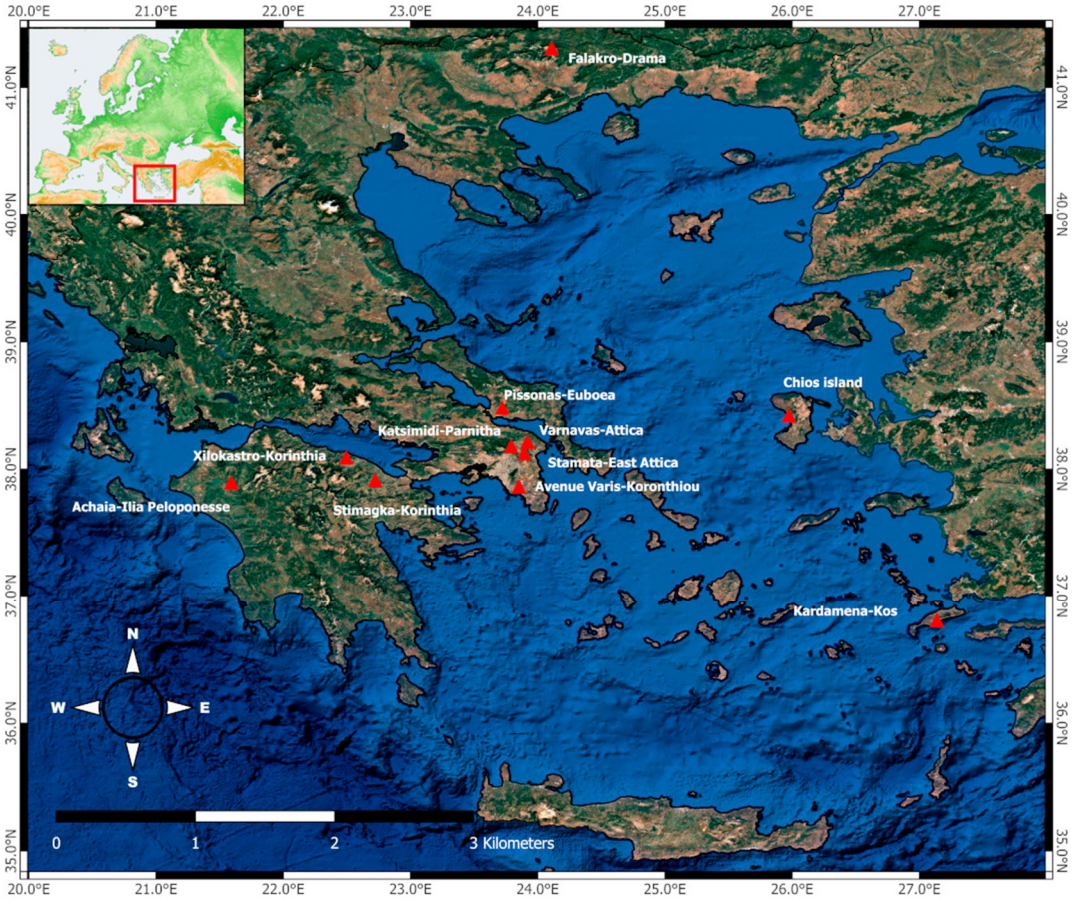

Figure 1. Map of Greece showing the locations of the 11 wildfires analyzed in this study, marked with red triangles.

Our objective is to evaluate how consistently such a multi-source approach characterizes severity patterns across fires with different landscape settings. We hypothesize that this integrated framework can produce stable severity classifications across multiple wildfire events and enhance the interpretation of landscape-dependent variations in burn severity, complementing the information provided by spectral indices.

2. Materials and Methods

Meteorological data were collected from the Hellenic National Meteorological Service, the European Drought Observatory, the Copernicus Atmosphere Monitoring Service, 2025, and Freemeteo [23–26] and compared to the fire risk models of the BEYOND Earth Observation Center's Daily Fire Risk Map Prediction platform [27]. As such, the climate data collected for the time of each fire case, along with the BEYOND fire risk scale, were used for a qualitative analysis of the event date.

The wildfires were mapped using two atmospherically corrected Sentinel-2 L2A satellite images for each fire—one taken before and the other after the event (Table 1). These images were processed using SNAP v.9 and ArcGIS v.10.8 software [28,29]. The preprocessing phase involved generating cloud masks, resampling the images to a 10 m resolution, and calculating the Normalized Burn Ratio (NBR) index. The main processing phase included calculating relevant indices, applying necessary corrections, and extracting

data to generate the final maps. A detailed overview of the methodological steps is provided in Figure 2.

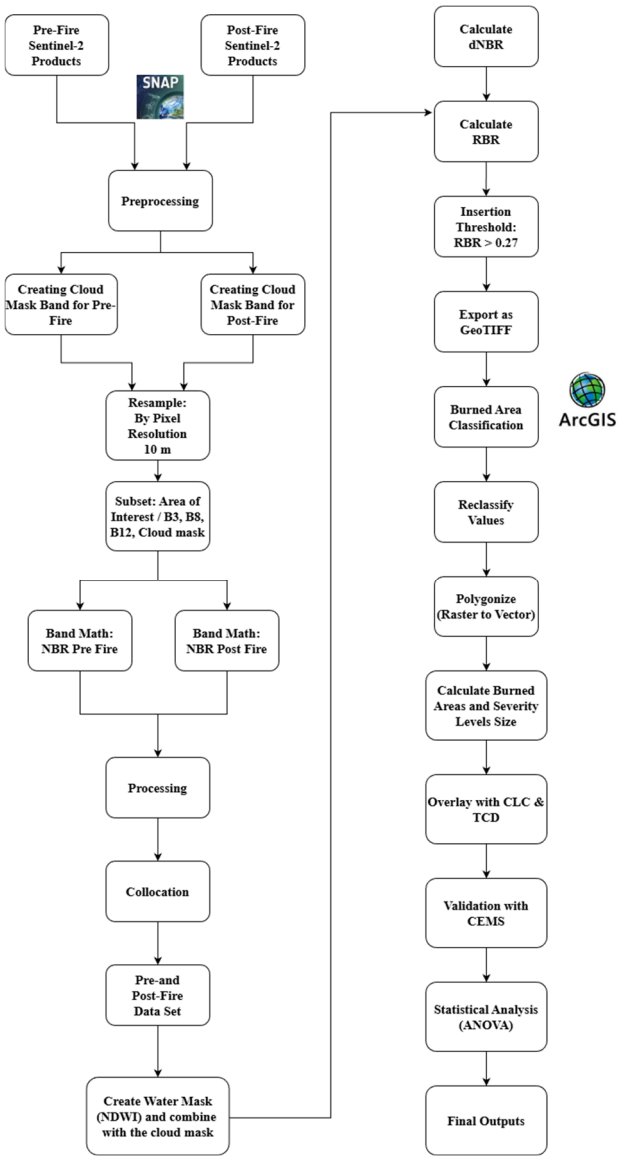

Figure 2. Flowchart of the methodology applied for wildfire analysis.

Table 1. Sentinel-2 images for each area.

Area	Wildfire Start Date	Sentinel-2 Acquisition Date
Avenue Varis–Koropiou	19 June 2024	18 June 2024 28 June 2024
Achaia–Ilia	21 June 2024	16 June 2024 26 June 2024
Katsimidi–Parnitha	29 June 2024	23 June 2024 8 July 2024
Stamata	30 June 2024	26 June 2024 8 July 2024
Metochi Sidirountas	1 July 2024	23 June 2024 13 July 2024

Table 1. *Cont.*

Area	Wildfire Start Date	Sentinel-2 Acquisition Date
Kardamena–Kos	1 July 2024	30 June 2024 5 July 2024
Stimagka–Korinthia	11 July 2024	1 July 2024 16 July 2024
Varnavas	11 August 2024	2 August 2024 17 August 2024
Falakro–Drama	17 July 2024	16 July 2024 28 July 2024
Pissonas–Evoia	31 July 2024	28 July 2024 2 August 2024
Xylokastro–Korinthia	29 September 2024	29 September 2024 4 October 2024

Preprocessing involved cloud masking and resampling of the Sentinel-2 bands to a consistent resolution of 10 m to match higher-resolution bands. After resampling, the images were clipped to the Region of Interest (ROI) and the NBR index was calculated to detect burned areas. For its calculation, the near-infrared (NIR) (Band 8, 0.842 nm wavelength) and shortwave-infrared (SWIR) (Band 12, 2.19 nm wavelength) bands are utilized, as outlined in Equation (1) [30].

$$\mathrm{NBR} = \mathrm{NIR} - \mathrm{SWIR}/\mathrm{NIR} + \mathrm{SWIR} \quad (1)$$

The NBR index ranges from −1 to 1, with lower values indicating burned areas [31]. Water bodies and clouds were masked out using a composite mask, and the Normalized Difference Water Index (NDWI) was applied to isolate water bodies (Equation (2)). GREEN channel is Band 3 of Sentinel-2 satellite images and NIR channel is Band 8 of Sentinel-2. Band 3 (GREEN) has a central wavelength (~560 nm) while Band 8 (NIR) has a central wavelength of 842 nm. This index is designed to maximize the reflectance of the water bodies in Green Band and is minimized in the NIR band [32].

$$\mathrm{NDWI} = (\mathrm{GREEN} - \mathrm{NIR})/(\mathrm{GREEN} + \mathrm{NIR}) \quad (2)$$

The difference in NBR values (dNBR) was calculated to identify recently burned areas and assess fire severity (Equation (3)).

$$\mathrm{dNBR} = \mathrm{PrefireNBR} - \mathrm{PostfireNBR} \quad (3)$$

The RBR was then calculated to refine burn severity evaluations, using masks to remove cloud and water interference [33]. The RBR index was first proposed by Parks et al. [34] and the goal was to invent an alternative, more reliable burn severity metric. RBR is a relativized version of dNBR and more improved in several aspects, such as classification accuracy and avoidance of mathematical difficulties. RBR ranges from −1 to 1.3. Values close to 0 indicate unburned areas, negative values indicate vegetation increase, and positive values over 0.1 indicate burned areas. Higher values of RBR indicates regions with higher burn severity. The above classification follows the United States Geological Survey (USGS) guidelines [35,36]. These indices are commonly used for wildfire mapping and provide a consistent framework for assessing fire severity across land cover types.

$$RBR = dNBR/(NBRpre + 1.001) \quad (4)$$

Final results were visualized in ArcGIS v. 10.8 [29] using thresholds established by the United States Geological Survey (USGS) to categorize burn severity (low, moderate, high). Areas with RBR values between 0.1 and 0.27 were categorized as low severity. Moderate–low severity areas had RBR values ranging from 0.27 to 0.439, while moderate–high severity regions fell between 0.44 and 0.659. Lastly, high-severity regions were categorized by values from 0.66 to 1.3. After the classification procedure, the burn area was then vectorized to calculate the extent of the burned areas. The CORINE Land Cover (CLC) 2018 dataset and Tree Cover Density (TCD) data were extracted to assess damage [37,38].

CLC data provide pan-European land cover and land use with 44 thematic classes. This dataset is updated and has a new status added every 6 years, with the latest version made in 2018. The CLC dataset has a Minimum Mapping Unit of 25 hectares for areal phenomena and a Minimum Mapping Width of 100 m for linear phenomena [37,39].

TCD data are raster-type data at 10 m resolution. TCD represents the proportion of a pixel covered by tree canopies for the region of Europe. The range is between 0% and 100%. As with the CLC dataset, TCD datasets are widely utilized for monitoring forest areas and observing any changes. The data used are shown in Table 2.

Table 2. Exploited data.

Data	Format	Resolution	Source
Sentinel-2 Imagery	Optical Level–2A	10 m	Dataspace Ecosystem Copernicus
CORINE Land Cover	Vector (Polygon)	–	Copernicus Land Monitoring Service
Tree Density	Raster	10 m	Copernicus Land Monitoring Service

Burn area estimations were validated by comparing the results with Copernicus Emergency Management Service (CEMS) datasets. The aim of CEMS datasets is the effective rapid mapping of fire-affected regions at both a European and global level [40]. By utilizing the percentage of overlap between the burned area estimated by our team and the CEMS, validation accuracy was carried out. Afterwards, results were characterized as overestimated or underestimated according to overlap percentages. In the case of overestimation, validation accuracy was estimated, as CEMS reported the burned area divided by the affected area our team estimated. On the contrary, in the underestimation cases, validation accuracy was carried out by dividing the burned area our team calculated by the CEMS reported affected area. CEMS products are widely used for fire mapping and have shown strong agreement with Sentinel-2-based fire extent estimates, confirming their suitability for validation in this study [41].

ANOVA is a commonly applied statistical technique used to assess whether the mean values of three or more groups differ significantly [42]. The method incorporates two primary sources of variability: (i) between-group variance, which measures how much the group means diverge from the overall mean, and (ii) within-group variance, which reflects the degree of variability among observations belonging to the same group [43]. A one-way ANOVA was performed to examine whether the distribution of burned area among the predefined severity levels showed systematic differences. In this study, the ANOVA serves as a quantitative complement to the mapped severity patterns, providing

a numerical description of how the classified severity levels are represented in terms of burned surface area.

The independent variable was Severity Level, consisting of four groups: Low Severity, Moderate–Low Severity, Moderate–High Severity and High Severity. Burned area (in km^2) served as the dependent variable. Prior to running ANOVA, descriptive statistics were generated for each severity group using SPSS software v.30.0 [44], thus facilitating the execution of the statistical analysis [45]. These included measures of central tendency (mean, median, trimmed mean), dispersion (variance, standard deviation, range, interquartile range), and skewness and kurtosis, along with the 95% confidence intervals for the mean. This descriptive output ensured an initial understanding of data structure and facilitated verification of the normality and homogeneity assumptions. Normality within each severity class was evaluated using skewness and kurtosis values, supported by visual inspection of histograms and Q–Q plots.

3. Results

3.1. Burn Severity

Burn severity was estimated for each wildfire to understand its impact and aid in preventing future catastrophic events. The spatial distribution of burn severity revealed distinct patterns among the studied cases. In Varis–Koropiou (Table 3, Figure 3), the burned area was predominantly characterized by low to low–moderate severity, reflecting limited vegetation damage and relatively mild fire behavior. Conversely, the Ilia and Stamata wildfires exhibited a more heterogeneous severity distribution, with a considerable proportion of the area classified within moderate severity levels, indicative of more extensive ecological impact. The Katsimidi case demonstrated the highest burn severity, with moderate to high–moderate categories prevailing across most of the affected area. These results are consistent with the influence of local environmental conditions, such as vegetation density, fuel continuity, and topography, shaping the spatial organization of burn severity patterns.

Table 3. Severity of the burn area.

	Avenue Varis–Koropiou	**Achaia–Ilia**	**Katsimidi, Parnitha**	**Stamata**
Severity	Percentage (%)	Percentage (%)	Percentage (%)	Percentage (%)
Low	52.47	32.67	15.47	28.41
Moderate–low	47.05	40.40	48.30	63.36
Moderate–high	0.48	26.93	36.29	8.24
High	–	–	–	–
Total burnt area	0.82 km^2	40.55 km^2	0.66 km^2	1.41 km^2

Across the four study areas, burn severity patterns varied notably. Kardamena and Stimagka were dominated by moderate to high burn severities, indicating relatively intense fire effects, whereas Falakro and Metochi showed a greater extent of low to low–moderate severity, suggesting less severe impacts on vegetation (Table 4, Figure 4). In Kardamena and Stimagka, over 70% of the burned area fell within the moderate to high severity classes, while Falakro was largely characterized by moderate–low severity (over 60%). Metochi exhibited the most balanced distribution, with low and low–moderate classes together accounting for roughly 80% of the burned area. Overall, these patterns reflect differing fire behaviors and landscape responses across sites, likely influenced by variations in vegetation type, topography, and pre-fire conditions.

Table 4. Severity of the burn area.

	Kardamena–Kos	Metochi–Chios	Stimagka–Korinthia	Falakro–Drama
Severity	%	%	%	%
Low	21.69	39.44	30.92	29.51
Moderate–low	41.90	40.44	29.86	63.37
Moderate–high	36.40	20.11	39.08	7.12
High	–	0.005	0.13	–
Total burnt area	5.07 km^2	10.84 km^2	6.34 km^2	13.79 km^2

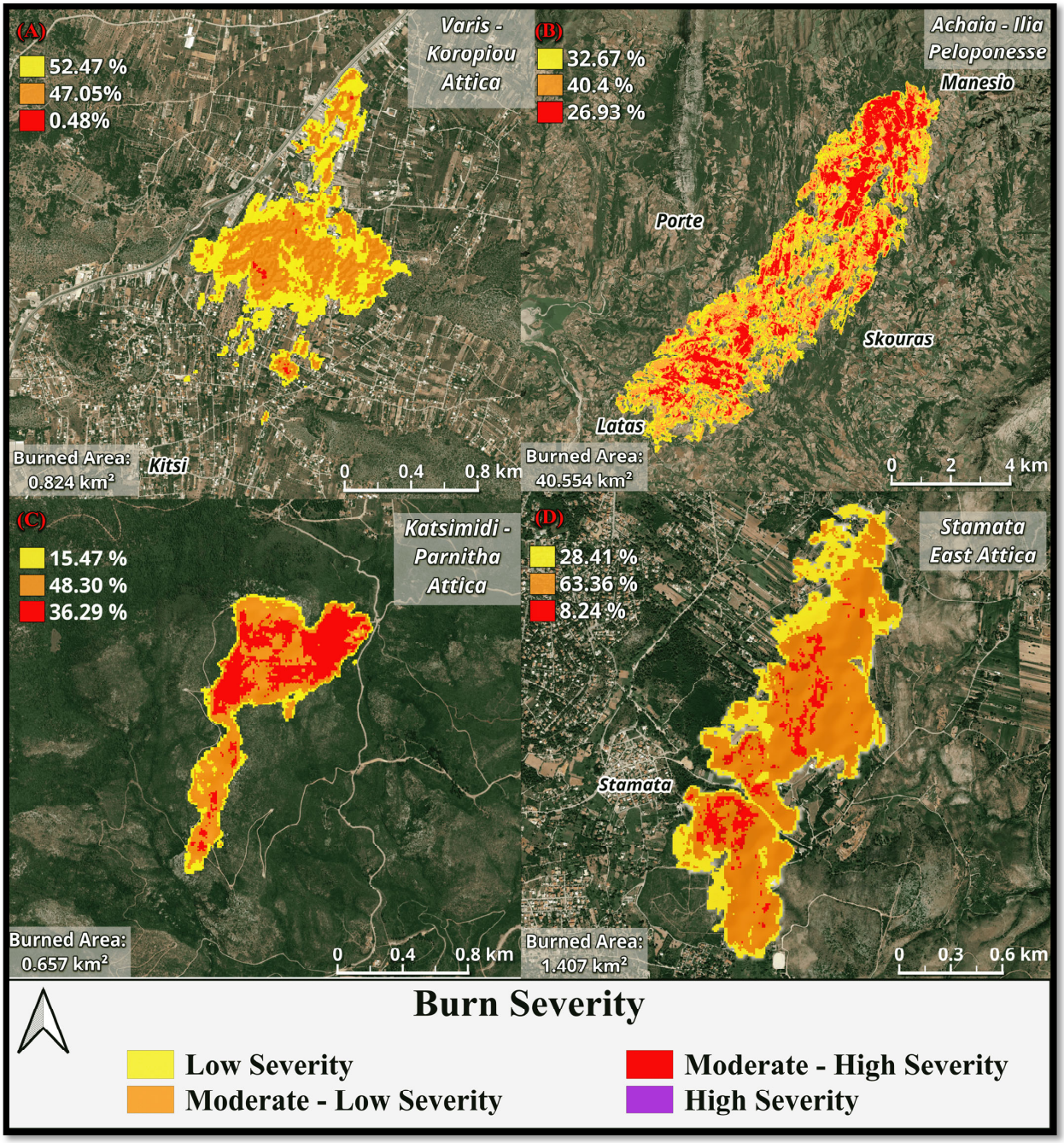

Figure 3. Burn severity maps for the Varis–Koropiou (**A**), Achaia–Ilia (**B**), Katsimidi–Parnitha (**C**), and Stamata (**D**) wildfires, showing the distribution of low, moderate–low, moderate–high, and high-severity areas.

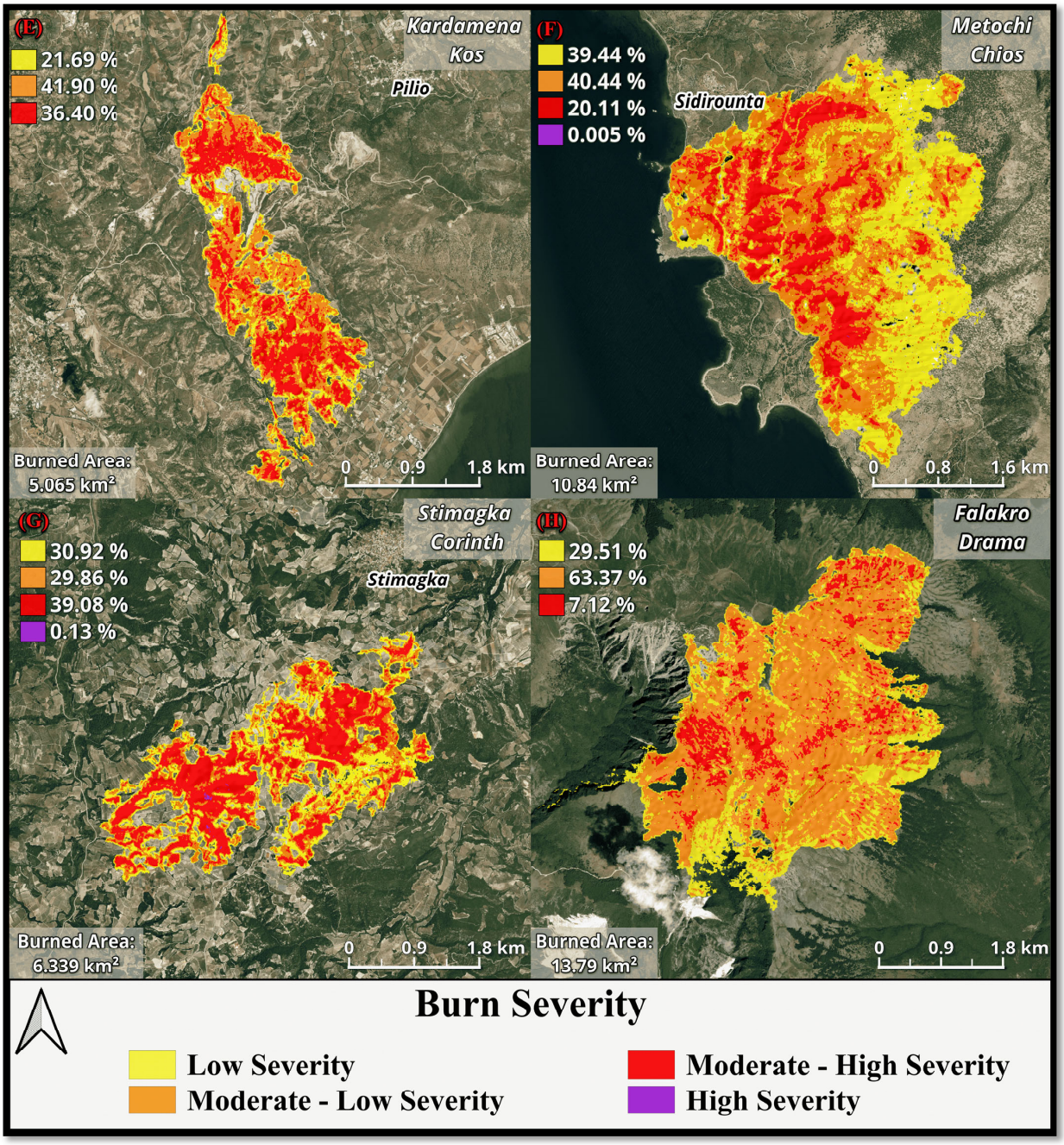

Figure 4. Burn severity maps for the Kardamena (**E**), Chios (**F**), Stimagka (**G**), and Falakro (**H**) wildfires, showing the distribution of low, moderate–low, moderate–high, and high-severity areas.

The Pissonas, Varnava, and Xylokastro cases exhibited distinct burn severity patterns, reflecting differences in fire intensity and landscape characteristics (Table 5, Figure 5). The Varnava wildfire was by far the most severe, with over half of its burned area classified as moderate-to-high severity, indicating extensive vegetation loss and intense burning. Pissonas also showed a predominance of moderate–high severity, though with a more balanced distribution across severity levels compared to Varnava. In contrast, Xylokastro presented a more even mix of low, moderate–low, and moderate–high severities, with only a minimal area affected by high severity. Overall, these patterns suggest that while Varnava experienced the most destructive fire conditions, Pissonas and Xylokastro exhibited more moderate fire impacts, possibly influenced by differences in fuel continuity, topography, and local microclimates.

Table 5. Severity of the burn area.

	Pissonas–Euboea	Varnavas	Xylokastro–Korinthia
Severity	%	%	%
Low	14.05	13.07	23.76
Moderate–low	36.11	31.17	37.46
Moderate–high	49.78	55.12	38.26
High	0.06	0.65	0.50
Total burnt area	9.81 km^2	106.77 km^2	67.03 km^2

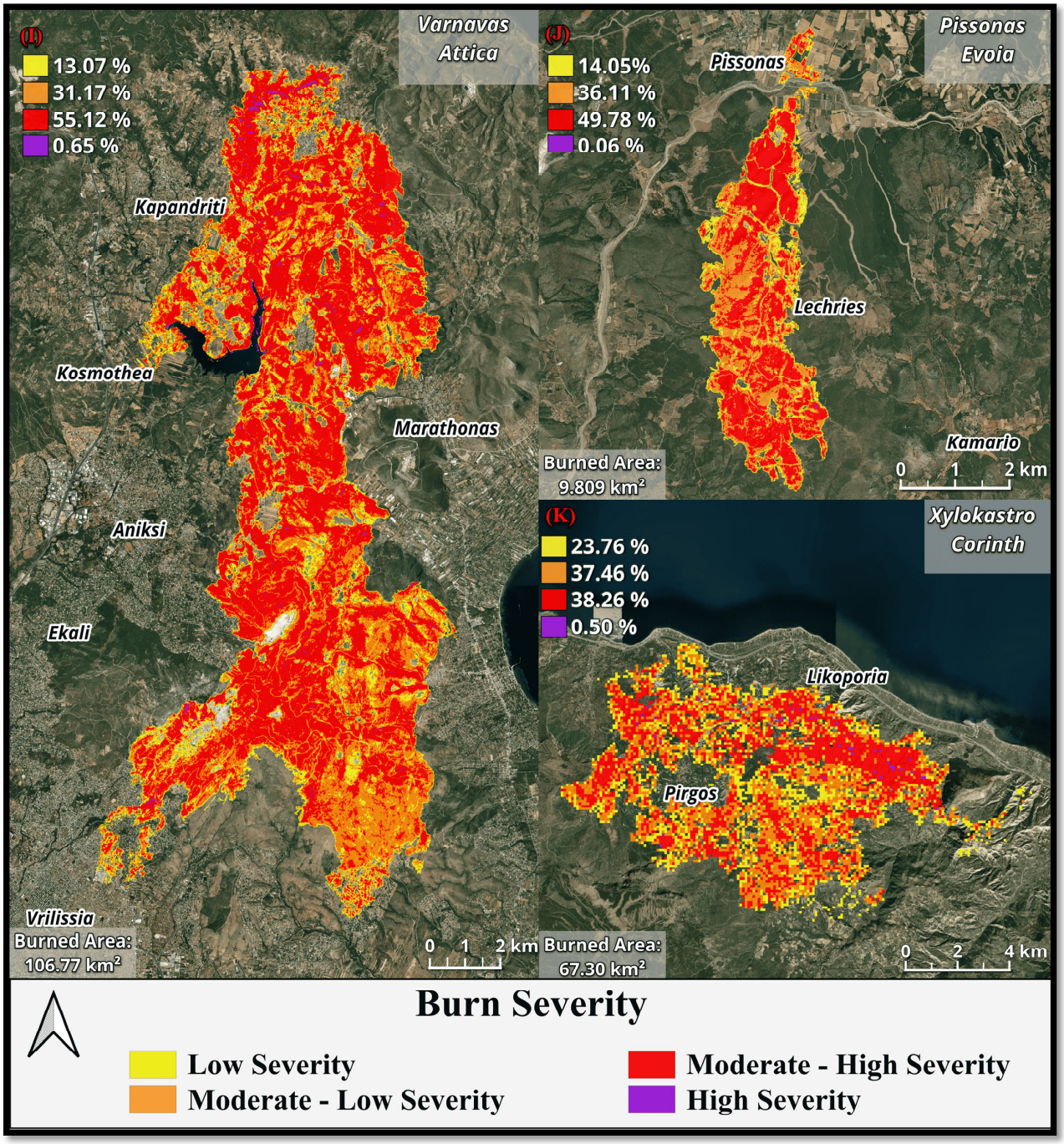

Figure 5. Burn severity maps for the Varnavas (**I**), Pissonas (**J**), and Xylokastro (**K**) wildfires, showing the distribution of low, moderate–low, moderate–high, and high-severity areas.

3.2. Corine Land Cover

The estimation of burn severity and the total area affected is not enough to fully assess the destruction caused by the fire. Therefore, the CLC 2018 database was used to better understand the type of land cover destroyed. The main CLC categories for each wildfire are shown in Table 6.

Table 6. Main CLC category for each wildfire analyzed.

	Main CLC Category	%	Total Burnt Area (km^2)
Avenue Varis–Koropiou	Sclerophyllous Vegetation	50.63	0.82
Achaia–Ilia	Land principally occupied by agriculture, with significant areas of natural vegetation	35.65	40.55
Katsimidi–Parnitha	Mixed forest	55.98	0.66
Stamata	Transitional woodland–shrub	62.43	1.41
Kardamena–Kos	Sclerophyllous Vegetation	49.90	5.07
Metochi–Chios	Transitional woodland–shrub	45.70	10.84
Stimagka–Korinthia	Transitional woodland–shrub	50.87	6.34
Falakro–Drama	Natural grasslands	91.85	13.79
Pissonas–Euboea	Transitional woodland–shrub	37.20	9.81
Varnavas	Transitional woodland–shrub	36.52	106.77
Xylokastro–Korinthia	Transitional woodland–shrub	39.03	67.03

For the Varis–Koropiou case (Figure 6), the most affected land type was sclerophyllous vegetation, covering 50.63% of the burnt area (~0.41 km^2). The second most affected was complex cultivation patterns (23.13%, 0.19 km^2). Smaller areas of discontinuous urban fabric and industrial commercial units were also affected, particularly along the south and northwest sides of the burnt area. In the Ilia wildfire case, land principally occupied by agriculture was the most affected category, covering 35.65% (~14.46 km^2). Sclerophyllous vegetation covered 28.52% (~11.57 km^2), as well as transitional woodland–shrub 15.37% (~6.23 km^2). The area affected by agriculture was predominantly agricultural land, with non-irrigated arable land (8.28%) and olive groves (0.07%) also impacted.

For the Katsimidi wildfire, most of the area was covered by mixed forest (55.98%, 0.37 km^2) and transitional woodland–shrub (44.01%, 0.29 km^2), with both categories spread across the northwest and southeast sides of the affected area. In the Stamata wildfire, similar to Varis–Koropiou, sclerophyllous vegetation and transitional woodland–shrub were the most impacted categories. Sclerophyllous vegetation covered 0.23 km^2 (~16.19%) and transitional woodland–shrub 0.88 km^2 (62.43%), with smaller areas of land principally occupied by agriculture (0.15 km^2) and complex cultivation patterns (0.13 km^2).

For the Kardamena wildfire (Figure 7), the affected land was primarily agricultural, with non-irrigated arable land covering 8.19% (0.41 km^2) and olive groves 4.30% (0.22 km^2). The most affected land types were sclerophyllous vegetation (2.53 km^2) and natural grassland (1.90 km^2). In the Metochi wildfire (Chios), the most impacted land types were transitional woodland–shrub (45.70%, 4.94 km^2) and sclerophyllous vegetation (31.91%, 3.45 km^2), followed by olive groves (0.44 km^2), natural grassland (0.78 km^2), and sparsely vegetated areas (1.16 km^2).

For the Stimagka wildfire, transitional woodland–shrub was the most affected (50.86%, 3.23 km^2), followed by vineyards (1.77 km^2) and land principally occupied by agriculture (0.56 km^2). The least impacted category was olive groves (0.34 km^2). In the Falakro wildfire,

the primary land type affected was natural grassland (91.85%, 12.45 km^2), followed by broad-leaved forest (7.45%, 1.01 km^2) and sparsely vegetated areas (0.7%, 0.09 km^2).

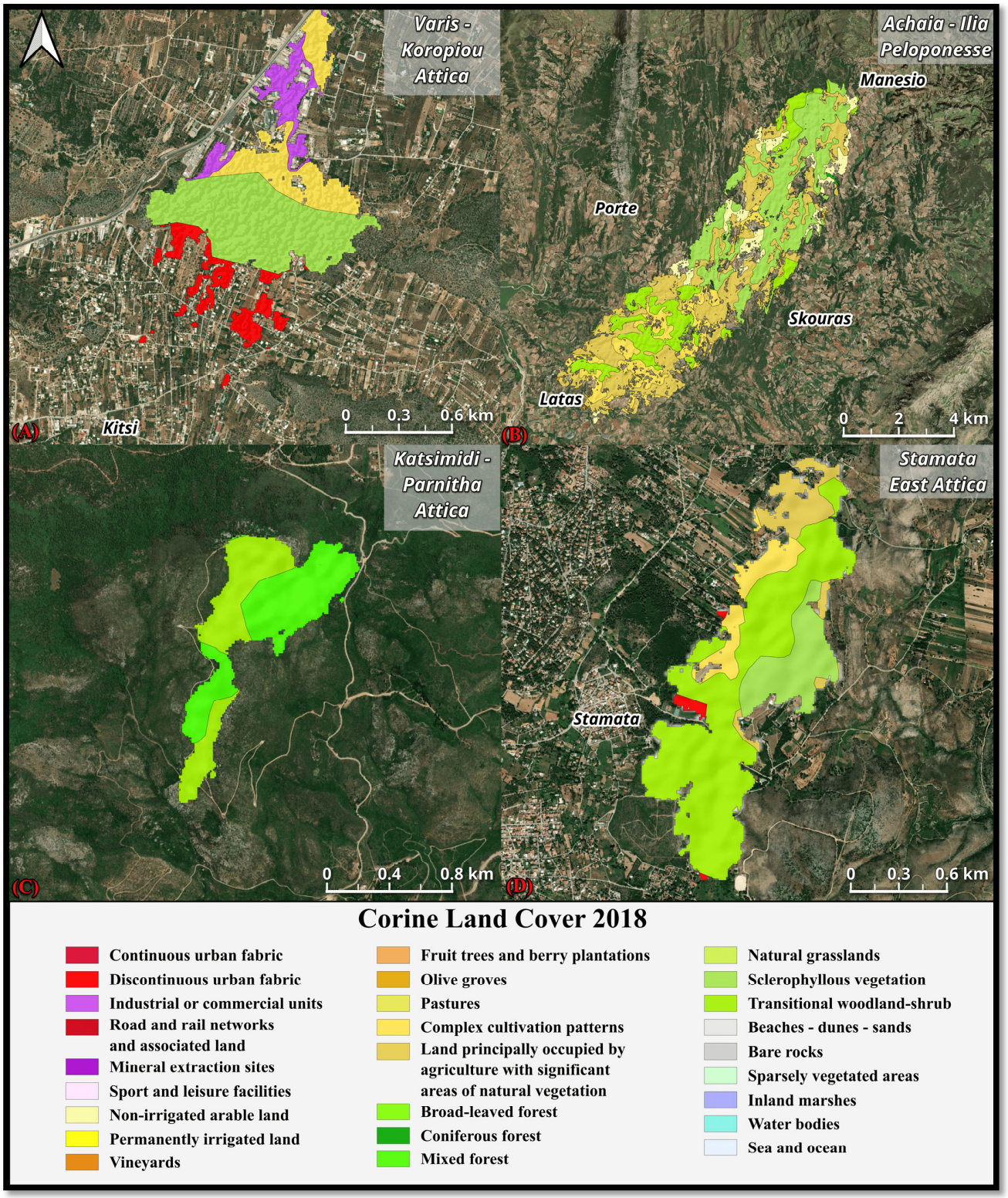

Figure 6. Land use maps for the Varis–Koropiou (**A**), Achaia–Ilia (**B**), Katsimidi–Parnitha (**C**), and Stamata (**D**) wildfires.

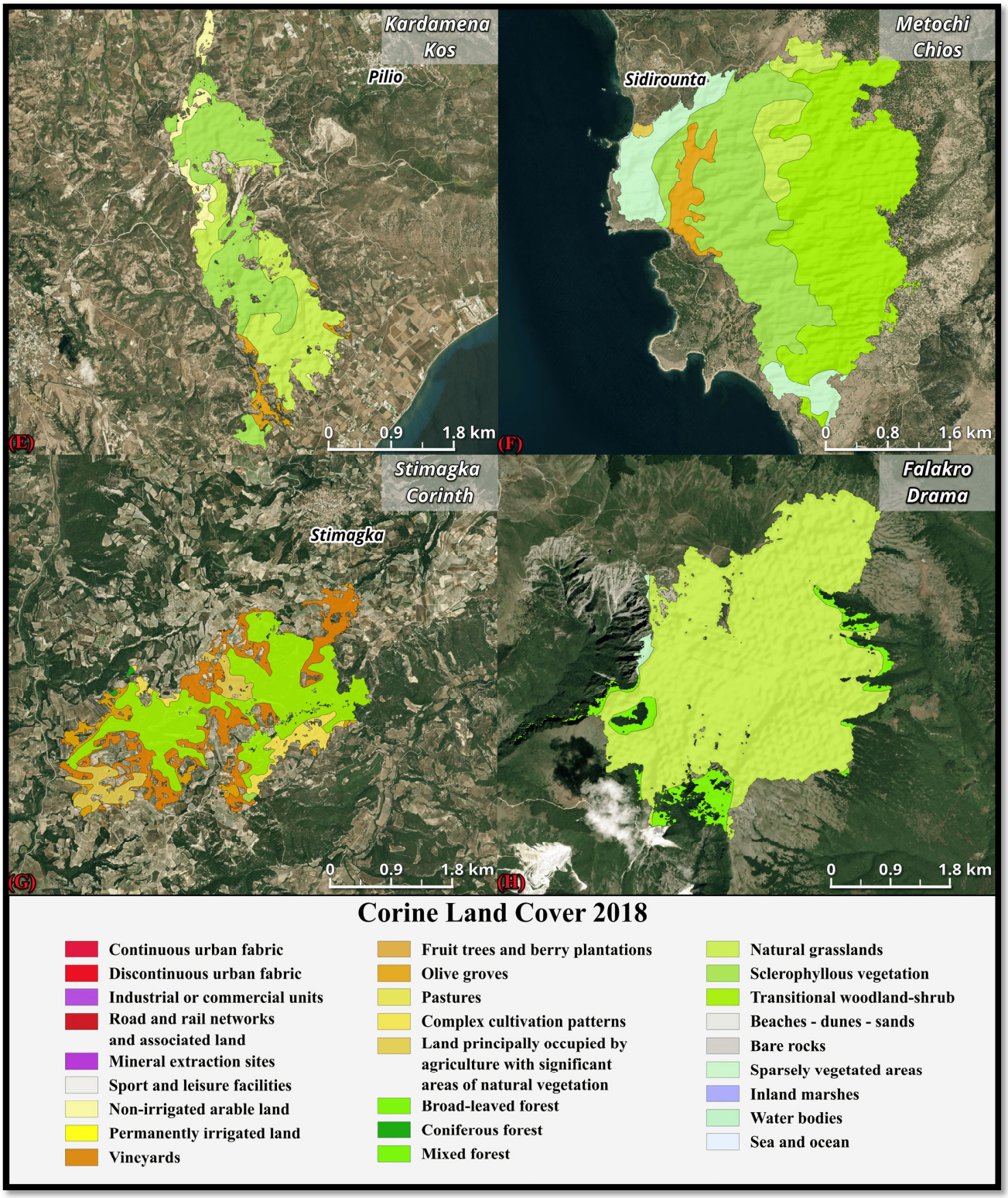

Figure 7. Land use maps for the Kardamena (**E**), Chios (**F**), Stimagka (**G**), and Falakro (**H**) wildfires.

Following the Varnavas wildfire case (Figure 8), the CLC results showed the greatest variety of affected categories. Four of these categories belong to the urban class, with discontinuous urban fabric being the most impacted, covering 3.94 km^2 (~3.63%), located on the south and north sides of the burned area. Mineral extraction covered 0.25 km^2 (~0.23%) in the northwest part of the area. Smaller urban areas, such as continuous urban fabric (0.1 km^2, ~0.10%) and sport or leisure facilities (0.003 km^2, ~0.002%), are located in

the outskirts. In terms of agricultural land, land principally occupied by agriculture was the most affected (9.10 km^2, ~8.37%), followed by complex cultivation patterns (6.24 km^2, ~5.75%) and non-irrigated arable land (3.26 km^2, ~3%). The largest impacted land type was transitional woodland–shrub, covering 39.68 km^2 (~36.52%), followed by sclerophyllous vegetation (26.86 km^2, ~24.72%). Smaller areas were affected by sparsely vegetated areas (16.09 km^2, ~14.8%) and other forest types like mixed forest and coniferous forest.

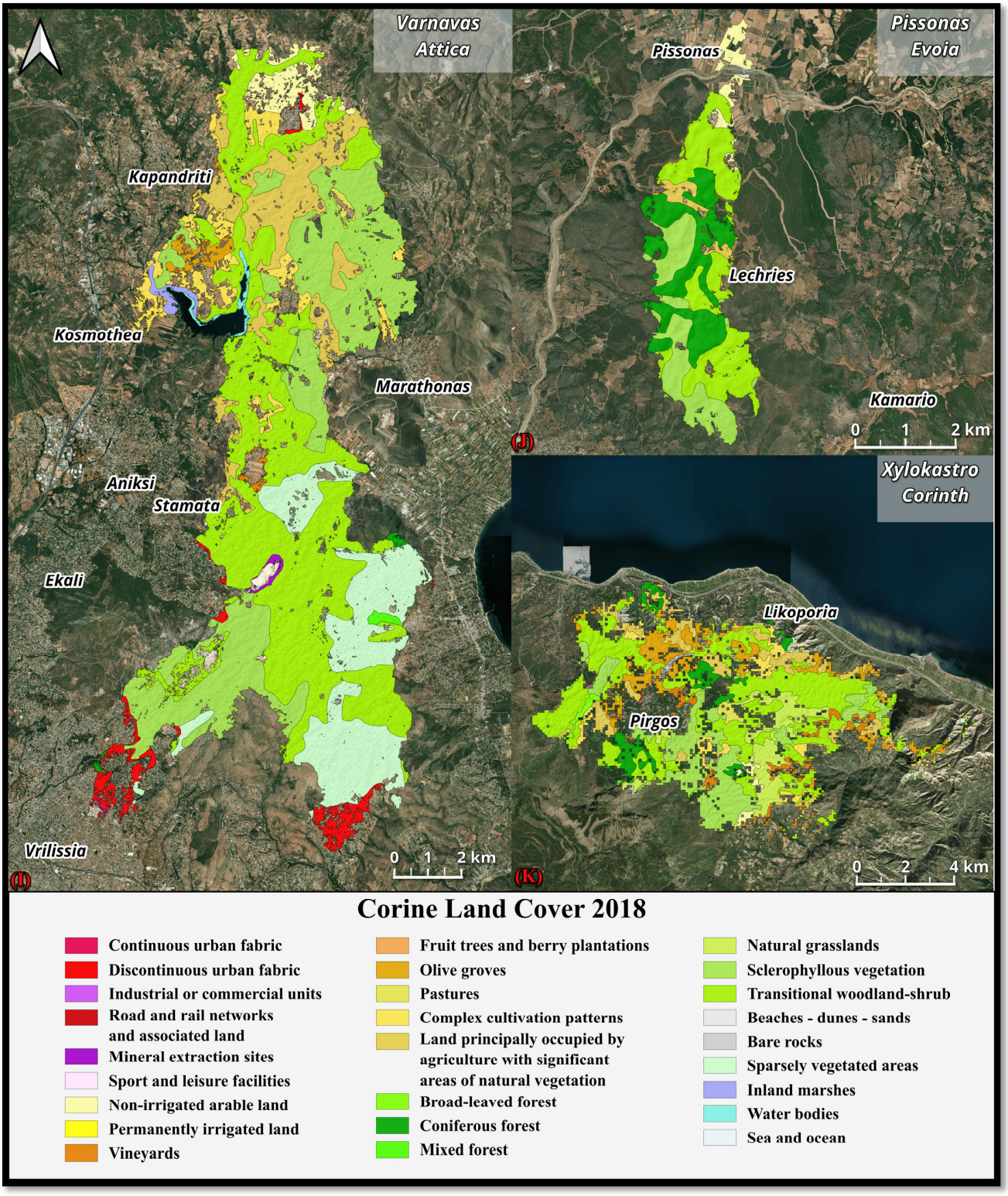

Figure 8. Burn severity maps for the Varnavas (**I**), Pissonas (**J**), and Xylokastro (**K**) wildfires.

For the Pissonas wildfire, transitional woodland–shrub was the largest affected category, covering 37.20% (3.65 km^2), followed by coniferous forest (28.76%, 2.82 km^2). Smaller areas were affected by sclerophyllous vegetation (23.63%, 2.32 km^2) and non-irrigated arable land (6.2%, 0.6 km^2). The Xylokastro wildfire primarily affected transitional woodland–shrub (39.03%, 26.31 km^2) and sclerophyllous vegetation (17.17%, 11.56 km^2), with smaller areas of olive groves (10.26%, 6.91 km^2) and land principally occupied by agriculture (9.49%, 6.39 km^2). Summarizing all cases, transitional woodland–shrub was the most affected land type, covering 32.24% (85.20 km^2) of the total burnt area, followed by sclerophyllous vegetation at 22.30% (58.94 km^2).

3.3. Tree Cover Density Results

The majority of the burnt areas analyzed are dominated by forested or agricultural land types. To accurately assess the wildfire's impact, TCD data was retrieved from Copernicus Land Services, providing a raster map divided into 10 density classes, from 1% to 10% (low density) to 90% to 100% (full tree cover). The main results of tree cover density are shown in Table 7.

Table 7. Main Tree Cover Density category for each wildfire analyzed.

	Main TCD Category	%	Total Burnt Area (km^2)
Avenue	1–10%	99.50	0.82
Varis–Koropiou	1–10%	42.15	40.55
Achaia–Ilia	90–100%	41.57	0.66
Katsimidi–Parnitha	1–10%	66.23	1.41
Stamata	1–10%	94.00	5.07
Kardamena–Kos	1–10%	65.04	10.84
Metochi–Chios	1–10%	62.50	6.34
Stimagka–Korinthia	1–10%	96.21	13.79
Falakro–Drama	1–10%	62.01	9.81
Pissonas–Euboea	1–10%	90.06	106.77
Varnavas	1–10%	65.73	67.03
Xylokastro–Korinthia			

In the Varis–Koropiou case (Figure 9), most of the affected area was classified as 1% to 10% tree density (99.50%, 0.82 km^2), with very small areas of 10–20% and 20–30% tree density. For the Achaia–Ilia wildfire, the most affected category was 1% to 10% tree density, covering 42.15% (17.125 km^2). The next most affected categories were 50–60% and 60–70%, covering 16.16% (6.566 km^2) and 17.84% (7.248 km^2), respectively. The 40–50% and 70–80% classes accounted for 9% (3.695 km^2) and 8.57% (3.48 km^2) of the area.

The Katsimidi wildfire was different, with 41.57% (0.270 km^2) of the area classified as 90–100% tree density and additional large portions classified in high-density categories (80–90%, 60–70%, 50–60%). Smaller areas had 30–40%, 20–30%, and 10–20% tree density. For the Stamata wildfire, the largest area (66.23%, 0.928 km^2) was in the 1% to 10% category. Other significant categories were 50–60% (14.63%, 0.205 km^2) and 40–50% (14.57, 0.205 km^2). Smaller areas were found in categories ranging from 60–70% to 70–80%.

The Kardamena wildfire (Figure 10) showed a dominant 1% to 10% tree density category (94%, 4.76 km^2). The next most affected were 40–50% (1.82%, 0.09 km^2) and 30–40% (1.64%, 0.08 km^2), with smaller portions in higher density classes. For Metochi, the majority (65.04%, 7.048 km^2) was in the 1% to 10% category. The next most affected were 30–40% (10.66%, 1.156 km^2) and 40–50% (8.24%, 0.892 km^2). Smaller areas were classified as 10–20%, 50–60%, and 60–70%.

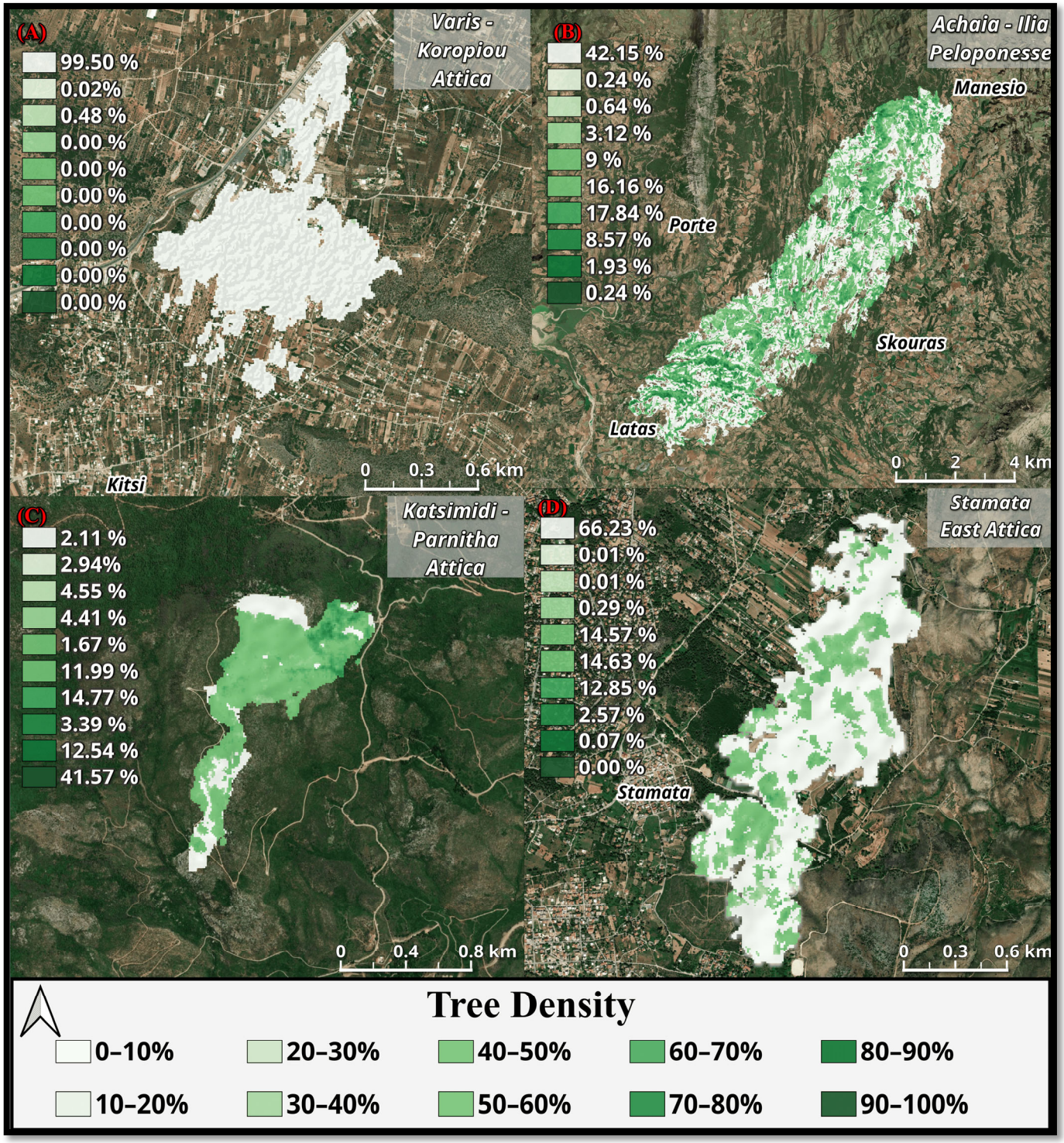

Figure 9. Tree Cover Density maps for the Varis–Koropiou (**A**), Achaia–Ilia (**B**), Katsimidi–Parnitha (**C**), and Stamata (**D**) wildfires. The color gradient ranges from lightest green/white (0–10%) to darkest green (90–100%), indicating the proportion of the area covered by trees.

The Stimagka case showed a broad variety of TCD classes. The majority (62.49%, 3.963 km^2) was in the 1% to 10% category, followed by 50–60% (12.4%, 0.786 km^2) and 40–50% (10.21%, 0.648 km^2). The Falakro wildfire mirrored the Varis–Koropiou case, with 96.21% (13.251 km^2) in the 1% to 10% category. The remaining area was covered by smaller percentages in the 60–70%, 50–60%, and 70–80% categories.

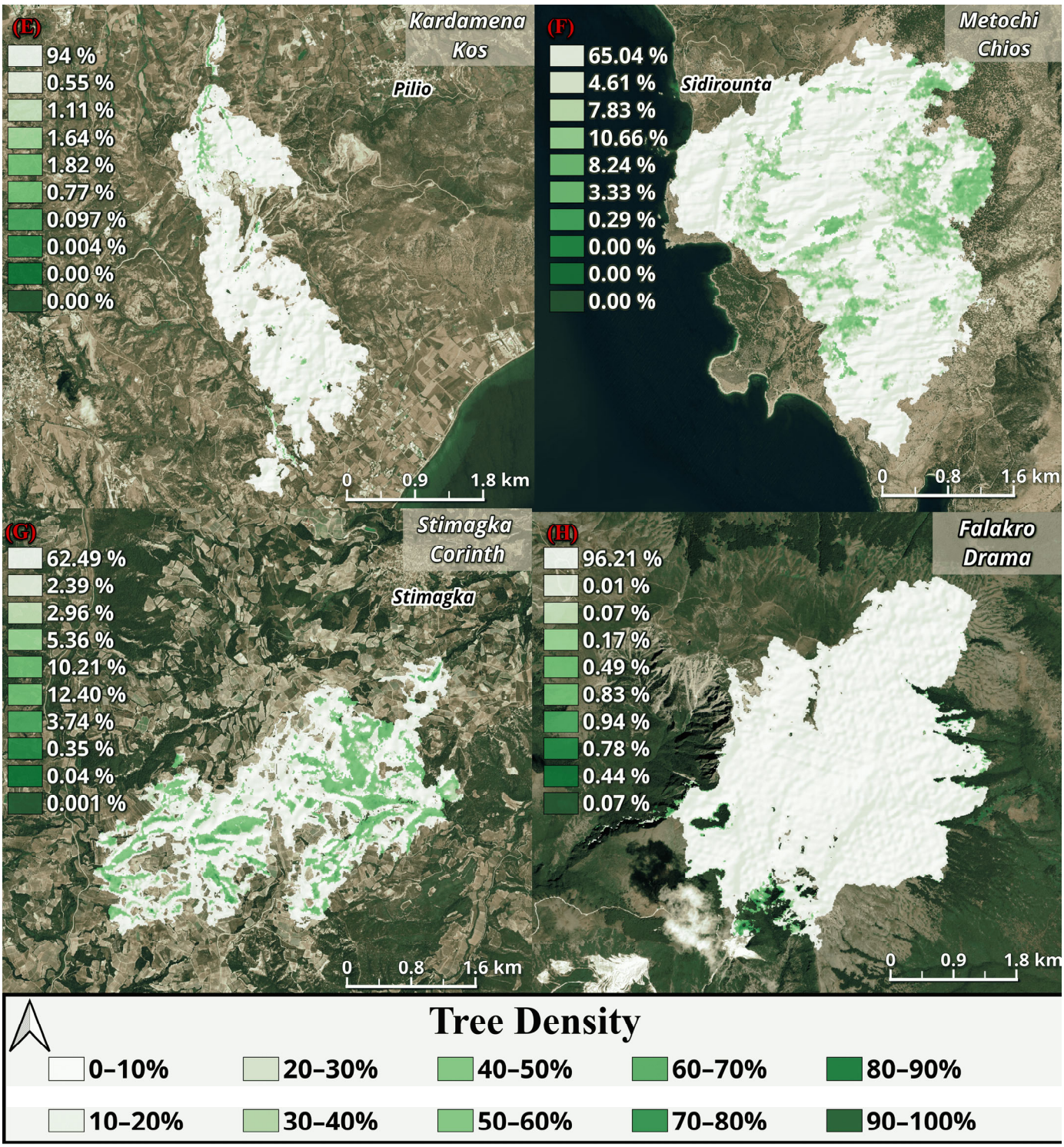

Figure 10. Tree Cover Density maps for the Kardamena (**E**), Chios (**F**), Stimagka (**G**), and Falakro (**H**) wildfires.

For the Varnava wildfire (Figure 11), the largest portion (90.06%, 98.52 km^2) was in the 1% to 10% class, followed by 50–60% (2.34%, 2.56 km^2). Other categories with lower coverage included 60–70% and 30–40%. The Pissonas wildfire showed a similar pattern to Stamata and Achaia–Ilia, with 62% (6.204 km^2) in the 1% to 10% class. Other notable categories included 30–40% (19.29%, 1.928 km^2) and 20–30% (12.29%, 1.229 km^2). In the

Xylokastro case, 65.73% (44.24 km^2) was classified in the 1% to 10% category, with significant portions in the 40–50% (9.79%, 6.59 km^2) and 50–60% (7.77%, 5.23 km^2) categories.

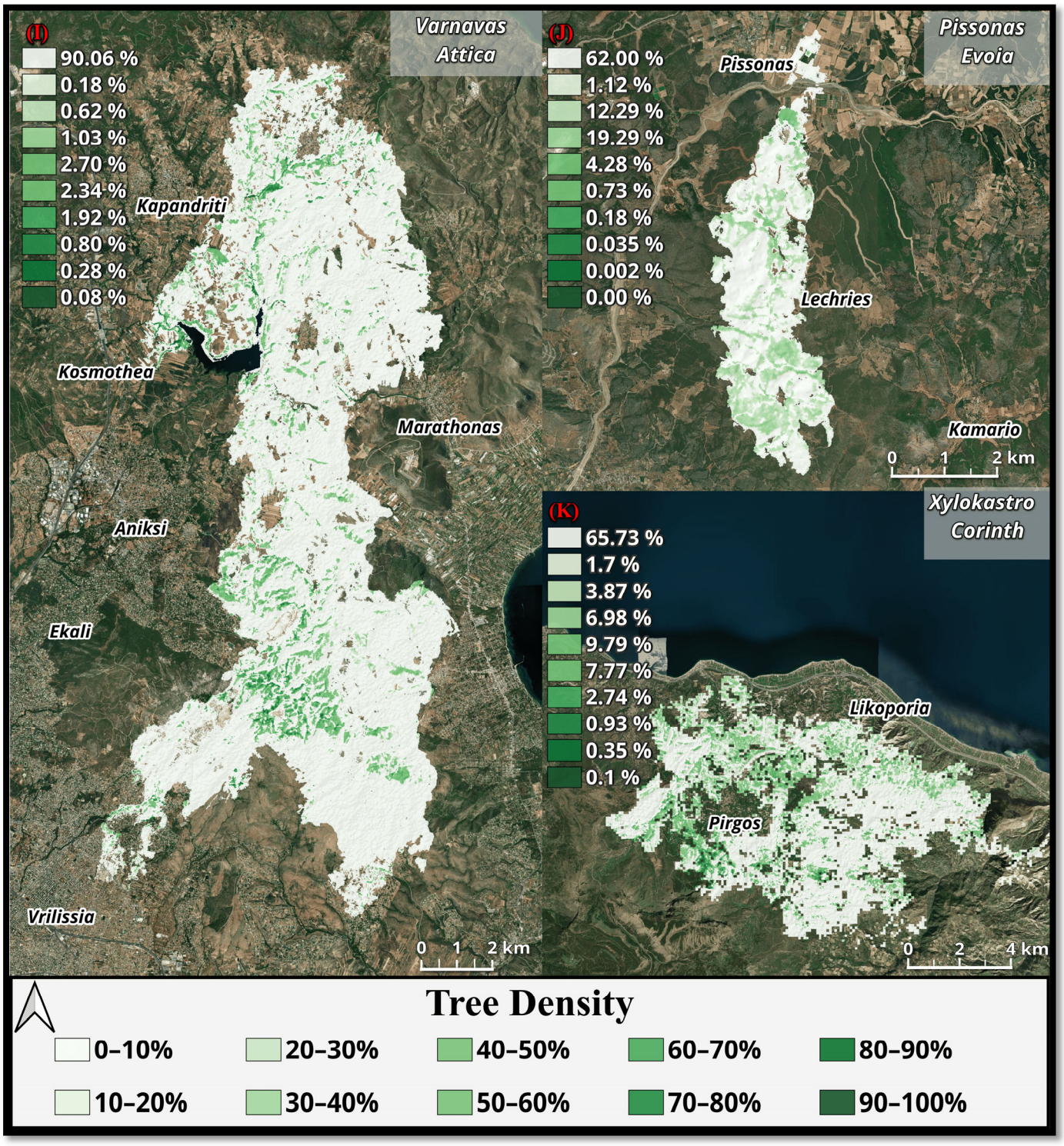

Figure 11. Tree Cover Density maps for the Varnavas (**I**), Pissonas (**J**), and Xylokastro (**K**) wildfires.

3.4. Fire Starting Conditions

This research aims to assess potential correlations between climatic conditions and fire risk on the days of wildfire occurrences.

The Varis–Koropiou fire on June 19th, 2024, occurred with a temperature of 35.3 °C, humidity 21%, and wind speed of 6 Bf (Table 8). The area faced drought conditions with

314 h of sunshine, and air quality was affected by Saharan dust. BEYOND assessed this period as Very High Risk. For the Achaia–Ilia fire on 21 June 2024, the temperature reached 38.9 °C, with humidity 32% and wind speeds of 3 Bf. The region had drought conditions with 345 h of sunshine, and the fire risk was deemed Very High.

Table 8. Fire starting conditions for the Varis–Koropiou, Achaia–Ilia, Katsimidi–Parnitha, and Stamata wildfires.

	Avenue Varis–Koropiou	Achaia–Ilia	Katsimidi–Parnitha	Stamata
High Temperature (°C)	35.3	38.9	20.7	29.6
Mean Temperature (°C)	31.7	30.7	17.6	26.2
Humidity (%)	21	32	25	21
Wind velocity (Bf)	6	3	5	7
Sunshine duration (h/M)	314	345	–	–
Precipitation (mm)	–	–	0	0
Air quality	Saharan dust	Saharan dust	Saharan dust	Saharan dust
Drought conditions	warning drought conditions	warning drought conditions	34 days-long drought	warning drought conditions
Fire Risk	Very High Risk	Very High Risk	Very High Risk	Very High Risk

The Katsimidi fire on 29 June 2024 had a temperature of 20.7 °C and wind speeds of 5 Bf. The area was under drought for 34 days, with Saharan dust and humidity ranging from 21 to 54%. The fire risk was Very High. On 30 June 2024, the Stamata fire occurred with a temperature of 29.6 °C and wind speeds of 7 Bf. The humidity was at 21%, and Saharan dust was present. The fire risk was assessed as High to Very High.

The analysis of the 2024 summer wildfires in Kardamena, Metochi, Stimagka, and Falakro revealed distinct meteorological contexts that influenced fire behavior. In all cases, high temperatures and moderate winds prevailed, while precipitation was absent, indicating persistent dryness despite signs of drought recovery (Table 9). Relative humidity generally remained low, reinforcing the flammability of the vegetation. Notably, BEYOND's fire danger assessments did not always align with the actual fire occurrences, as several events (e.g., Stimagka and Falakro) took place under conditions categorized as low or very low fire risk. This discrepancy suggests that local microclimatic effects and fuel conditions may have played a critical role, emphasizing the need for refined fire risk models that incorporate finer-scale environmental variables.

Table 9. Fire starting conditions for the Kardamena, Chios, Stimagka, and Falakro wildfires.

	Kardamena–Kos	Metochi–Chios	Stimagka–Korinthia	Falakro–Drama
High Temperature (°C)	30	33.1	31.6	39.7
Mean Temperature (°C)	27.6	29.1	26.7	30.8
Humidity (%)	43	57	18	24
Wind velocity (Bf)	5	3	4	3
Sunshine duration (h/M)	–	352	–	351
Precipitation (mm)	0	0	0	0.2
Air quality	–	–	–	–
Drought conditions	recovery or normal conditions.	recovery or normal conditions.	recovery or normal conditions.	recovery or normal conditions.
Fire Risk	High–Medium Risk	Very High Risk	Very Low Risk	Very Low Risk

The Pissonas fire on 31 July 2024 occurred with temperatures of 32.1 °C and wind speeds of 4 Bf (Table 10). The humidity was 20% and no precipitation was recorded throughout the period. The fire risk was Very High. The Varnava wildfire on 11 August 2024 had a temperature of 29.8 °C, wind speeds of 5 Bf, and humidity of 32%. Lastly, the Xylokastro fire on 29 September 2024 had temperatures of 29.1 °C, wind speeds of 1 Bf, and humidity of 58%. The fire risk was Medium.

Table 10. Fire starting conditions for the Varnavas, Pissonas, and Xylokastro wildfires.

	Pissonas–Euboea	**Varnavas**	**Xylokastro–Korinthia**
High Temperature (°C)	32.1	29.8	29.1
Mean Temperature (°C)	28.8	26.7	23.7
Humidity (%)	20	32	58
Wind velocity (Bf)	4	5	1
Sunshine duration (h/M)	–	–	–
Precipitation (mm)	0	0	0
Air quality	–	–	–
Drought conditions	recovery or normal conditions	alert drought conditions	warning drought conditions
Fire Risk	Very High Risk	Very High Risk	Medium Risk

3.5. ANOVA

The results showed that the Mean Burnt Area exhibits substantial variation across the severity levels. The Moderate–Low Severity group reports the highest mean (43.58), while the High Severity group presents the lowest mean (3.81). This distribution reflects clear structural differences in how the burned area is represented across the severity levels and offers a concise quantitative summary of the severity composition of the analyzed wildfires. The means Low Severity (27.40) and Moderate–High Severity (28.89) are statistically similar, indicating comparable contributions of these classes to the overall burned surface. The relationship between the Mean and the Median provides initial insight into skewness. Skewness coefficients quantify the degree to which a data distribution deviates from perfect symmetry [46,47].

Descriptive statistics reveal distinct burnt area distributions across fire severity groups, directly supporting ANOVA's identification of significant between-groups differences. High Severity exhibits extreme right-skewness (mean = 3.81, median ≈ 0.05), with most fires affecting small areas and rare large events increasing spatial variability. The Low Severity group displays near symmetry (mean ≈ median), reflecting uniform small-scale burned areas. Moderate–Low Severity shows a mild right skew (mean > median), driven by occasional larger fires, while Moderate–High Severity indicates a left skew (median > mean), with clustered smaller burns. Variability is highest in Moderate–High Severity (SD ≈ 17.93, variance ≈ 321.56) and lowest in Moderate–Low (SD ≈ 11.29, variance ≈ 127.55); High Severity's low IQR (0.50) confirms central data clustering amid outliers, linking to ecological fire regime patterns.

Spearman's rank correlation was conducted at the fire-event scale (N = 11) to examine the relationship between relative humidity and area weighted burn severity. Spearman's rank correlation coefficient ranges from −1 to +1, with values close to +1 indicating a perfect positive monotonic relationship, values close to −1 indicating a perfect negative monotonic relationship, and values near zero indicating no monotonic association [48]. The analysis revealed a weak positive association (ϱ = 0.251); however, the correlation was not statistically significant (p = 0.456), indicating that relative humidity alone does not strongly influence burn severity among the analyzed fire events. Several studies have shown that topographic variables are relatively more influential in determining high burn severity than

vegetation and meteorological factors, as topography strongly affects fire behavior, fuel moisture, water balance, and the spatial distribution and productivity of vegetation [49,50].

Influence of meteorological factors on burn severity is not uniform and may vary both among different fire events and within individual fires [51]. Furthermore, wind has a dual effect on wildfire behavior, enhancing fire spread at moderate speeds while potentially limiting fire effects at very high velocities through disruption of fuel continuity [52].

3.6. Validation of the Burned Areas

The validation of the burned areas from the analysis was carried out using open-access post-fire measurements from the CEMS Mapping. CEMS provides two types of products: Rapid Mapping, published shortly after the disaster, and Risk and Recovery Mapping, focused on long-term disaster management. Rapid Mapping products were used to validate the results in this study, offering detailed information on the burned areas [53].

Rapid mapping products, such as those of CEMS, have been used in the past as a reference for burn area delineation and burn severity mapping [41,54]. Additionally, comparisons to such products have been utilized as a method of validation in multiple occasions in recent studies. More specifically, Kovacs [55] compared his fire severity results, estimated through the RBR index, with the CEMS burn severity products based on the 2018 Kineta and Mati cases in Greece. Similarly, when studying the fires of 2017 in the Iberian Peninsula, Llorens et al. [56] validated their dNBR burn severity results by comparing them with various products, including the CEMS burn severity values. Colomba et al. [57] utilized the CEMS burn severity products as a reference during their collection of Sentinel-2 satellite data, as well as when applying the severity classification. Lastly, Donezar-Hoyos et al. [58] performed an evaluation of the validation process of CEMS fire products. As is evident by these studies, comparison of estimated burn severity indices and burn area delineation with CEMS fire products is a common practice and can be a robust form of research validation.

Burned area estimations from this study and CEMS Mapping were compared. The Varis–Koropiou fire (19 June 2024) showed an accuracy of 98.05%, with the study reporting 0.82 km^2 and CEMS reporting 0.8 km^2. For the Achaia–Ilia wildfire (21 June 2024), the study estimated 40.55 km^2, while CEMS reported 38.66 km^2, achieving an accuracy of 95.35%. The Katsimidi fire was reported by the study at 0.65 km^2, and CEMS at 0.64 km^2, leading to a high accuracy of 99.38%. For the Stamata fire, the study estimated 1.4 km^2 and CEMS reported 1.3 km^2, resulting in an accuracy of 92.86%.

The Kardamena wildfire (Kos) showed the lowest accuracy, with the study estimating 5.06 km^2 and CEMS at 4.39 km^2, yielding an accuracy of 86.92%. The Metochi wildfire in Chios was estimated at 10.84 km^2, with CEMS reporting 10.39 km^2 (95.85% accuracy). The Stimagka fire had the lowest accuracy (84.68%), with the study estimating 6.33 km^2 and CEMS reporting 5.36 km. The Falakro wildfire had perfect accuracy, with both the study and CEMS reporting 13.79 km^2.

Pissonas Euboea had nearly perfect accuracy (99%), with the study estimating 9.8 km^2 and CEMS reporting 9.704 km^2. The Varnava wildfire was the largest of 2024, with the study estimating 106.77 km^2 and CEMS reporting 104.14 km^2, achieving 97.53% accuracy. The Xylokastro wildfire showed a lower accuracy (86.63%), with the study estimating 67.3 km^2 and CEMS reporting 58.29 km^2.

In total, the study estimated the burned area for all fires analyzed in Greece during summer 2024 to be 263.31 km^2, while CEMS Mapping reported 247.49 km^2, giving an overall accuracy of 93.99%.

4. Discussion

Greece has experienced extraordinary fire seasons in 2007, 2021, and 2023, breaking historical records in area burned and severity [59]. This increase coincides with the rise of severe fires in the Mediterranean, directly linked to climate change and land-use changes [60]. The 2024 fires, like those of 2023 [61], occurred during periods of elevated temperatures and intense winds, conditions that have been associated in previous studies with rapid fire development in Mediterranean environments. Our results are consistent with these studies and they indicate that several of the 2024 fires took place under warm and dry atmospheric conditions similar to those documented in other recent Mediterranean fire seasons (e.g., 2021 and 2022 in southern Europe [62]).

The distribution of burn severities in the 11 Greek fires mirrors patterns found in other Mediterranean studies. In most cases, the majority of burned areas were of low to low–moderate severity, with high-severity areas being small or absent. This pattern is further supported by our ANOVA results, which confirmed that low–moderate severity classes accounted for significantly larger burned areas compared to the other severity categories.

This is consistent with previous Mediterranean fires, where low and moderate severity often dominate due to the mosaic structure of Mediterranean landscapes and the prevalence of vegetation types that typically burn at lower severities. For example, Dosiou et al. [61] reported that less than 5% of the burned area suffered extreme damage, with moderate damage predominating. Similarly, Saulino et al. [63] found that dNBR/RBR indices typically classify most Mediterranean burned areas as low to moderate severity.

4.1. Spatial Patterns and Severity as a Function of Climate, Land Cover, and Tree Density

The forest fires analyzed exhibited spatial patterns of severity linked to climatic and land-use factors. Most fires started under extreme conditions: high temperatures, low humidity, and strong winds well above local averages (Tables 8–10). These conditions favored rapid fire spread and intense behavior [64]. For example, many fires started during heatwaves, which reduced vegetation moisture, increasing the speed of spread. Our results coincided with high temperatures and winds, even in cases with relatively high humidity, where extreme heat and wind favored fires to spread.

Fires that affected Mediterranean forests (pine forests, dense holm oak forests) displayed more spatially continuous zones of higher severity, whereas fires burning in shrublands, crops, or pastures presented a mosaic of severities with significant areas of low severity. These patterns are consistent with that vegetation type and TCD strongly influence fire severity. High TCD (closed forests) coincided with high severity, relating to crown fires and high canopy mortality [63], while low TCD areas were affected primarily in the understory, resulting in lower burn severity.

Land cover influences severity, as shown by studies in other Mediterranean regions. In Italy, pre-fire land cover was found to be the most important factor in burn severity [63]. Similarly, TCD served as a good predictor of fire severity, with closed forests showing higher severity. In our multi-event assessment, areas with higher TCD tended to present higher severity values, whereas low-TCD areas more often corresponded to lower severity classes, supporting the consistency of these relationships across the 2024 fires.

Topography also played a role in fire spread [65,66]. In our study, topographic conditions provide useful spatial context for interpreting the distribution of mapped severity levels. In the Achaia–Ilia fire, steeper terrain corresponded with more continuous areas of mapped higher severity, whereas fires near inhabited areas (e.g., Varis–Koropiou, Katsimidi–Parnitha) showed more fragmented severity patterns. While the influence of suppression activities, accessibility and urban proximity cannot be isolated in this study, these observations are consistent with well-documented interactions between topography,

land-use context, and fire impacts in wildland–urban interface settings [67]. The spatial patterns observed across the study area reflect the combined influence of vegetation structure, topographic configuration, and the meteorological conditions during each event.

The ANOVA analysis leads to the conclusion that the Moderate–Low Severity category is associated with the largest average burned area. This quantitative result aligns closely with the general severity structure observed across the eleven fires and is consistent with broader patterns documented in Mediterranean and Western North American fire regimes. Baker et al. [68] reported that low to moderate severity fires accounted for approximately 85–98% of historical fire occurrences in several reconstructed landscapes, while Sakulich et al. [69] noted that extensive burned areas frequently correspond to surface fires of low to moderate severity, even when fuel loads are locally high. The predominance of these severity levels in terms of burned area therefore reflects characteristic burn patterns already described in the literature and reinforces the spatial observations derived from the Sentinel-2 severity maps.

Visual inspection of the Q–Q plots (Figure 12) for burned area across the four severity categories indicates that the data generally follow the expected normal distribution, with some deviations depending on severity level. For the Low Severity and Moderate–Low Severity groups, most points lie close to the reference line, suggesting that burned area values in these categories approximate normality reasonably well, with only minor deviations at the distribution tails. The Moderate–High Severity group also shows a broadly linear pattern, indicating that the distribution is suitable for a comparative analysis of means. The High Severity category displays the largest deviation from normality, with clusters of low values and a few high outliers. This behavior is consistent with the limited spatial extent of high-severity patches and supports the interpretation that strongly skewed burned-area distributions are characteristic of small, concentrated zones of high-severity fire effects.

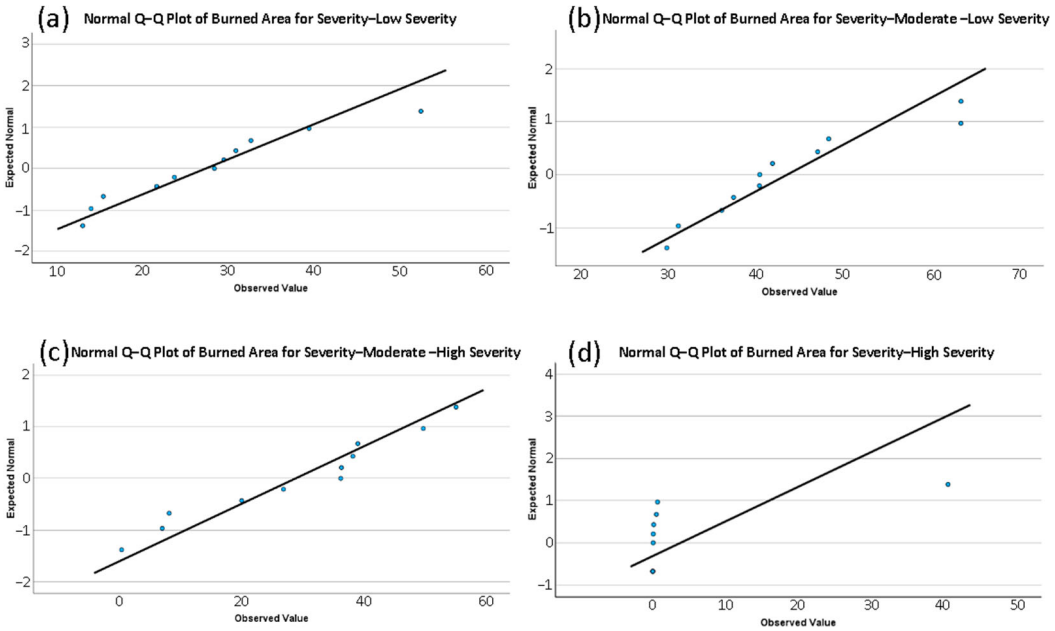

Figure 12. Normal quantile–quantile (Q–Q) plots illustrating the distribution of burned area values within each severity category: Low Severity (**a**), Moderate–Low Severity (**b**), Moderate–High Severity (**c**), and High Severity (**d**). Each plot compares the observed burned area values to the expected quantiles under a normal distribution.

4.2. Evaluation of the Methodology

The methodological contribution of this study lies in the consistent application of an integrated multi-source workflow across eleven wildfire events within a single fire season. This approach combines spectral severity indices, land-cover datasets, tree-density information, statistical analysis, and independent operational validation into a unified and replicable framework. This integration enables direct inter-event comparability and strengthens the interpretative capacity of burn-severity mapping in heterogeneous Mediterranean landscapes.

The multispectral remote sensing approach with spectral severity indices has proven effective in characterizing the analyzed fires. Sentinel-2 imagery was a key advantage in this study, offering higher spatial resolution (10 m) compared to other free and readily accessible alternatives and rapid revisit times. This is especially true for bands 3 and 8, although band 12 required resampling in order to match the 10 m resolution. The combination of NBR and dNBR indices provided a robust view of fire severity. The dNBR index was used to quantify spectral changes due to burning, following the USGS classification system for fire severity. These thresholds are determined through the integration of remote sensing data, specifically the NBR derived from satellite data. The classification thresholds are subsequently refined via statistical analysis and may be calibrated according to the prevailing vegetation types and ecosystem-specific attributes [16]. Integration of auxiliary data, such as CLC and TCD, enriched the analysis. CLC allowed us to estimate which cover types were most affected, contextualizing fire severity with land use. TCD contributed to interpreting how severity varied across different forest structures, highlighting contrasts between densely forested areas and more open landscapes.

This approach aligns with recent recommendations to combine satellite imagery with biophysical landscape data for comprehensive fire impact assessments. Malandra et al. [67] demonstrated that including land cover and anthropogenic factors improves models of fire severity in large-scale Mediterranean fires. Our results support the usefulness of this integrated approach, showing that high-severity patches frequently coincided with continuous forest stands with higher TCD, whereas agricultural areas and grasslands generally corresponded to lower severity classes, suggesting rapid, low-intensity fires.

Validation with CEMS products provided confidence in the methodology. Comparing our burned area maps with CEMS delineations yielded an overall accuracy of 95–96%. This high agreement indicates that the Sentinel-2 processing workflow and the severity indices applied here produced spatial extents broadly consistent with independent operational products. Similar results were reported in 2023, with Dosiou et al. [61] showing over 96% overlap between dNBR-mapped areas and CEMS data. This confirms that our remote sensing methodology robustly reproduces the true extent of the fire damage, a crucial result given the impracticality of large-scale field validation in such extensive fires.

4.3. Implications for Risk Management

The findings of this study have practical implications for fire risk management and the development of prevention and recovery policies in Mediterranean environments. First, the occurrence of several fires during periods of elevated temperatures, strong winds, and low humidity highlights the relevance of integrating meteorological monitoring into operational prevention strategies. Although our analysis does not assess climatic drivers, the environmental conditions documented during the 2024 events are consistent with those identified in recent Mediterranean studies as critical for fire danger. This supports the need to improve early warning systems during critical weather events (heatwaves, strong winds, prolonged droughts) and adjusting firefighting resources proactively. The fact that large burned areas occurred even early in the season (May–June, [16]) also suggests that

defining the danger period with flexibility may be beneficial. Strengthening coordination between meteorological services and civil protection to implement temporary restrictions on high-risk activities (agricultural burning, machinery use in mountainous areas, etc.) is essential.

Second, the spatial relationship observed between land cover, TCD, and mapped severity patterns provides useful insights for land-use planning and vegetation management. Heterogeneous and mosaic-type landscapes tended to show more fragmented severity patterns, whereas continuous, densely forested areas more frequently corresponded to high-severity zones. This supports fire-smart landscape strategies, such as creating firebreaks through crops, pastures, or managed areas. Policies promoting agroforestry and extensive livestock farming can help maintain this mosaic landscape and reduce vulnerability to fire, counteracting the effects of rural abandonment that have increased fuel continuity in many Mediterranean regions. Previous studies have shown that the absence of agricultural and livestock activity has heightened fire risk, making fires more intense and harder to control [67,70].

In terms of post-fire conditions, the severity maps in this study are directly applicable to ecological recovery management. Areas mapped as Moderate–High or High severity can be prioritized for rehabilitation actions such as reforestation, erosion-control planting, or the installation of runoff barriers, whereas Low-severity areas are more likely to regenerate naturally. This enables a more efficient allocation of resources in post-fire restoration. The results also support long-term policy planning aimed at strengthening territorial resilience to wildfire. These include forest management plans incorporating fire frequency projections, community education programs on fire preparedness, and legal frameworks promoting territorial resilience. Additionally, the increasing availability of satellite data allows for continuous monitoring of fuel and vegetation water stress, which could be integrated into risk management agencies. This study highlights the usefulness of freely accessible remote sensing (Copernicus) for fire assessment.

4.4. Limitations of the Study and Future Lines of Research

While this study provides valuable insights, it is important to acknowledge its limitations and propose future research directions. First, the severity classification relied solely on spectral indices from Sentinel-2 images, without field validation. This approach assumes that spectral changes captured by dNBR and RBR correspond proportionally to ecological fire effects, although the strength of this relationship can vary across vegetation types and post-fire conditions. Studies have shown that the relationship between indices like dNBR and biophysical severity differs between forest types, such as coniferous, broad-leaved, or shrubland forests [71]. Future work should therefore focus on calibrating these indices for representative Mediterranean vegetation communities in Greece, which would enhance the ecological interpretability of severity maps. Nevertheless, wildfire studies frequently rely on remote-sensing-based validation approaches when systematic field campaigns are not feasible, e.g., [16,61]. In this study, the high level of agreement obtained with Copernicus Emergency Management Service burned-area products (~94%) provides additional confidence.

A second limitation concerns the spatial scope of the analysis, which focuses exclusively on eleven fires that occurred in Greece during the 2024 season. Expanding this study to include fires from multiple Mediterranean regions and years would help identify broader patterns and local exceptions. Comparative studies across countries (e.g., Spain, Italy, Algeria) and diverse years would assess the generalizability of our findings. Additionally, including socioeconomic factors (e.g., population density, accessibility, current

management policies) in multi-criteria studies could provide deeper insights into regional differences in fire severity.

5. Conclusions

This study assessed wildfire burn severity across eleven major fire events that occurred in Greece during the summer of 2024 through a consistent multispectral remote-sensing workflow based on Sentinel-2 imagery. The combined use of dNBR and RBR indices enabled a stable and comparable delineation of burn severity across heterogeneous landscapes. The results indicate that most burned areas were classified within the low to moderate–low severity categories, whereas high-severity patches were spatially limited and generally associated with densely forested areas exhibiting high Tree Cover Density. In contrast, shrublands, grasslands, and low-density vegetation landscapes were predominantly linked to lower severity levels, highlighting the strong influence of vegetation structure and land-cover configuration on fire impact patterns.

The integration of CORINE Land Cover and Tree Cover Density datasets provided an effective contextual framework for interpreting burn severity distribution within each fire perimeter. Transitional woodland–shrub formations and sclerophyllous vegetation repeatedly emerged as the most affected cover types, confirming their recurrent vulnerability within Mediterranean fire regimes. Meteorological descriptors at ignition time were typically characterized by elevated temperatures, low or moderate humidity, and the absence of precipitation. While these variables do not allow causal attribution, they consistently define the environmental setting under which the analyzed events developed.

Methodologically, the high level of agreement obtained with Copernicus Emergency Management Service burned-area products (overall accuracy $\approx 94\%$) confirms the reliability of the applied Sentinel-2-based workflow for rapid post-fire assessment. Beyond the specific results of the 2024 season, the main contribution of this study lies in the demonstration of a unified and replicable multi-source framework that integrates spectral indices, land-cover information, vegetation-structure metrics, statistical analysis, and independent operational validation across multiple wildfire events. This approach facilitates inter-event comparability and provides a scalable basis for future wildfire studies.

The findings offer practical value for wildfire prevention, recovery planning, and territorial management in Mediterranean environments. Severity maps derived from freely accessible satellite data can support prioritization of post-fire rehabilitation actions, including erosion-control measures, reforestation planning, and the identification of areas suitable for natural regeneration. Furthermore, the observed relationships between land cover, tree density, and severity patterns provide useful guidance for landscape management strategies aimed at reducing fuel continuity, promoting mosaic land use configurations, and strengthening fire-resilient territorial planning. At the policy level, the integration of remote-sensing-based severity monitoring into civil protection systems and environmental planning frameworks can enhance early-warning preparedness, optimize resource allocation, and contribute to evidence-based decision-making in increasingly fire-prone Mediterranean regions.

Author Contributions: Conceptualization, I.C.-M. and I.P.; methodology, E.B., I.A., E.-A.K., M.Z., I.-E.K. and A.T.; software, I.C.-M., E.B., I.A., E.-A.K., M.Z., I.-E.K. and A.T.; validation, I.C.-M., E.B., I.A., E.-A.K., M.Z., I.-E.K. and A.T.; formal analysis, I.C.-M., E.B., I.A., E.-A.K., M.Z., I.-E.K. and A.T.; investigation, I.C.-M., E.B., I.A., E.-A.K., M.Z., I.-E.K. and A.T.; resources, I.C.-M., E.B., I.A., E.-A.K., M.Z., I.-E.K. and A.T.; data curation, E.B., I.A., E.-A.K., M.Z., I.-E.K. and A.T.; writing—original draft preparation, I.C.-M., E.B., I.A. and I.P.; writing—review and editing, I.C.-M., E.B., I.A., E.-A.K., M.Z., I.-E.K., A.T. and I.P.; visualization, I.C.-M., E.B., I.A., E.-A.K., M.Z., I.-E.K. and A.T.; supervision,

I.C.-M. and I.P.; project administration, I.C.-M. and I.P. All authors have read and agreed to the published version of the manuscript.

Funding: This research received no external funding.

Data Availability Statement: The data used in this study consist of openly accessible Copernicus Sentinel-2 imagery available through the Copernicus Dataspace Platform https://dataspace.copernicus.eu/ (accessed on 24 November 2024).

Acknowledgments: The authors express their sincere gratitude to the National and Kapodistrian University of Athens for providing complimentary access to the SPSS software, which substantially supported the data analysis conducted in this study. The Department of Geography at Harokopio University of Athens is also gratefully acknowledged for offering the necessary facilities that enabled the completion of this work. Furthermore, the authors thank the European Space Agency for supplying the Sentinel-2 data used in this research.

Conflicts of Interest: The authors declare no conflicts of interest.

References

1. Tuel, A.; Eltahir, E.A. Why is the Mediterranean a climate change hot spot? *J. Clim.* **2020**, *33*, 5829–5843. [CrossRef]
2. Kotroni, V.; Bezes, A.; Dafis, S.; Founda, D.; Galanaki, E.; Giannaros, C.; Giannaros, T.; Karagiannidis, A.; Koletsis, I.; Kyros, G.; et al. Long–Term Statistical Analysis of Severe Weather and Climate Events in Greece. *Atmosphere* **2025**, *16*, 105. [CrossRef]
3. Intergovernmental Panel on Climate Change (IPCC). Mediterranean Region. In *Climate Change 2022–Impacts, Adaptation and Vulnerability*; Cambridge University Press: Cambridge, UK, 2023; pp. 2233–2272. [CrossRef]
4. Ferrelli, F. Remote Sensing applications for effective fire disaster management plans: A review. *Acad. Publ. Inf. Syst. Smart City* **2023**, *3*, 133. [CrossRef]
5. Kourtesiotis, C.; Liu, Q.; Philippopoulos, K.; Tzanis, C.; Matei, D.; Flocas, H. Internal climate variability and extreme temperatures over the Mediterranean. *Environ. Sci. Proc.* **2023**, *26*, 57. [CrossRef]
6. Peng, X.; Yu, M.; Chen, H.; Zhou, B.; Shi, Y.; Yu, L. Projections of wildfire risk and activities under 1.5 °C and 2.0 °C global warming scenarios. *Environ. Res. Commun.* **2023**, *5*, 031002. [CrossRef]
7. Garrido–Ruiz, C.; Sandoval, M.; Stolpe, N.; Sanchez–Hernandez, J.C. Fire impacts on soil and post fire emergency stabilization treatments in Mediterranean–climate regions. *Chil. J. Agric. Res.* **2022**, *82*, 335–347. [CrossRef]
8. Moya, D.; Alfaro-Sánchez, R.; López Serrano, F.; Dadi, T.; Hernández-Tecles, E.J.; Ferrandis, P.; De las Heras, J. Post-fire management of mediterranean forests: Carbon storage in regenerated areas in eastern Iberian Peninsula. *Cuad. Investig. Geogr.* **2014**, *40*, 371–386. [CrossRef]
9. Iliopoulos, N.; Aliferis, I.; Chalaris, M. Effect of Climate Evolution on the Dynamics of the Wildfires in Greece. *Fire* **2024**, *7*, 162. [CrossRef]
10. Mataix Solera, J. Alteraciones Físicas, Químicas y Biológicas en Suelos Afectados por Incendios Forestales: Contribución a su Conservación y Regeneración. Ph.D. Thesis, Universidad de Alicante, Alicante, Spain, 1999.
11. De Rigo, D.; Libertà, G.; Durrant, T.H.; Artés Vivancos, T.; San-Miguel-Ayanz, J. *Forest Fire Danger Extremes in Europe Under Climate Change: Variability and Uncertainty*; EUR 28926 EN; Publications Office of the European Union: Luxembourg, 2017.
12. Mataix–Solera, J.; Cerdà, A.; Arcenegui, V.; Jordán, A.; Zavala, L.M. Fire effects on soil aggregation: A review. *Earth-Sci. Rev.* **2011**, *109*, 44–60. [CrossRef]
13. Petropoulos, G.P.; Kontoes, C.; Keramitsoglou, I. Burnt area delineation from a uni–temporal perspective based on Landsat TM imagery classification using Support Vector Machines. *Int. J. Appl. Earth Obs. Geoinf.* **2011**, *13*, 70–80. [CrossRef]
14. Palaiologou, P.; Kalabokidis, K.; Day, M.A.; Kopsachilis, V. Evaluating socioecological wildfire effects in Greece with a novel numerical Index. *Fire* **2020**, *3*, 63. [CrossRef]
15. Chinamatira, L.; Mtetwa, S.; Nyamadzawo, G. Causes of wildland fires, associated socio–economic impacts and challenges with policing, in Chakari resettlement area, Kadoma, Zimbabwe. *Fire Sci. Rev.* **2016**, *5*, 1. [CrossRef]
16. Castro–Melgar, I.; Tsagkou, A.; Zacharopoulou, M.; Basiou, E.; Athinelis, I.; Katris, E.A.; Kalavrezou, I.-E.; Parcharidis, I. Wildfires During Early Summer in Greece (2024): Burn Severity and Land Use Dynamics Through Sentinel–2 Data. *Forests* **2025**, *16*, 268. [CrossRef]
17. Kumar, D.; Shankar, A. Novel remote sensing technologies for natural hazard management. *Environ. Sci. Pollut. Res.* **2024**, *31*, 53743–53748. [CrossRef] [PubMed]
18. Castro-Melgar, I.; Falaras, T.; Basiou, E.; Parcharidis, I. Assessment of the October 2024 Cut-Off Low Event Floods Impact in Valencia (Spain) with Satellite and Geospatial Data. *Remote Sens.* **2025**, *17*, 2145. [CrossRef]

19. Basiou, E.; Castro-Melgar, I.; Kranis, H.; Karavias, A.; Lekkas, E.; Parcharidis, I. Assessment of the Ground Vulnerability in the Preveza Region (Greece) Using the European Ground Motion Service and Geospatial Data Concerning Critical Infrastructures. *Remote Sens.* **2025**, *17*, 327. [CrossRef]
20. Castro-Melgar, I.; Gatsios, T.; Prudencio, J.; Ibanez, J.M.; Lekkas, E.; Parcharidis, I. Volcano Monitoring: Using SAR Interferometry for the Pre-Unrest of La Palma and the Post-Unrest of Santorini. In *Remote Sensing for Geophysicists*; CRC Press: Boca Raton, FL, USA, 2025; pp. 440–459. [CrossRef]
21. Kalavrezou, I.E.; Castro-Melgar, I.; Nika, D.; Gatsios, T.; Lalechos, S.; Parcharidis, I. Application of time series INSAR (SBAS) method using sentinel-1 for monitoring ground deformation of the Aegina Island (Western Edge of Hellenic Volcanic Arc). *Land* **2024**, *13*, 485. [CrossRef]
22. Kurbanov, E.; Vorobev, O.; Lezhnin, S.; Sha, J.; Wang, J.; Li, X.; Cole, J.; Dergunov, D.; Wang, Y. Remote sensing of forest burnt area, burn severity, and post–fire recovery: A review. *Remote Sens.* **2022**, *14*, 4714. [CrossRef]
23. Hellenic National Meteorological Service. Climate Bulletins and Studies 2025. Available online: https://emy.gr/en/bulletins-studies (accessed on 26 August 2025).
24. European Drought Observatory. Current Drought Situation in Europe. 2025. Available online: https://joint-research-centre.ec.europa.eu/european-and-global-drought-observatories/current-drought-situation-europe_en (accessed on 26 August 2025).
25. Copernicus Atmosphere Monitoring Service. Copernicus: Saharan Dust Strongly Affects Air Quality in Eastern Mediterranean. 2025. Available online: https://atmosphere.copernicus.eu/copernicus-saharan-dust-strongly-affects-air-quality-eastern-mediterranean (accessed on 27 August 2025).
26. Freemeteo. Daily History. 2025. Available online: https://freemeteo.gr/ (accessed on 30 August 2025).
27. National Observatory of Athens. Daily Fire Risk Map Prediction. BEYOND Center of Excellence. 2025. Available online: https://riskmap.beyond-eocenter.eu/ (accessed on 15 September 2025).
28. SNAP v.9 European Space Agency. SNAP Tool. Earth Observation Portal. Available online: https://earth.esa.int/eogateway/tools/snap (accessed on 10 September 2024).
29. Esri. ArcGIS v.10.8. 2020. Release 10.8. 1. Environmental Systems Research Institute: Redlands, CA, USA, 2020.
30. Garcia, M.J.L.; Caselles, V. Mapping burns and natural reforestation using thematic mapper data. *Geocarto Int.* **1991**, *6*, 31–37. [CrossRef]
31. Falaras, T.; Tselka, I.; Papadopoulos, I.; Nikolidaki, M.; Karavias, A.; Bafi, D.; Petani, A.; Krassakis, P.; Parcharidis, I. Operational Mapping and Post—Disaster Hazard Assessment by the Development of a Multiparametric Web App Using Geospatial Technologies and Data: Attica Region 2021 Wildfires (Greece). *Appl. Sci.* **2022**, *12*, 7256. [CrossRef]
32. McFeeters, S.K. The use of normalized difference water index (NDWI) in the delineation of open water features. *Int. J. Remote Sens.* **1996**, *17*, 1425–1432. [CrossRef]
33. Arisanty, D.; Feindhi Ramadhan, M.; Angriani, P.; Muhaimin, M.; Nur Saputra, A.; Puji Hastuti, K.; Rosadi, D. Utilizing Sentinel-2 Data for Mapping Burned Areas in Banjarbaru Wetlands, South Kalimantan Province. *Int. J. For. Res.* **2022**, *1*, 7936392. [CrossRef]
34. Parks, S.A.; Dillon, G.K.; Miller, C. A New Metric for Quantifying Burn Severity: The Relativized Burn Ratio. *Remote Sens.* **2014**, *6*, 1827–1844. [CrossRef]
35. Keely, J.E. Fire intensity, fire severity and burn severity: A brief review and suggested usage. *Int. J. Wildland Fire* **2009**, *18*, 116–126. [CrossRef]
36. Rozario, P.F.; Madurapperuma, B.D.; Wang, Y. Remote Sensing to Detect Burn Severity Risk Zones in Palo Verde National Park, Costa Rica. *Remote Sens.* **2018**, *10*, 1427. [CrossRef]
37. Corine Land Cover (CLC 2018). Copernicus Land Monitoring Service. Available online: https://land.copernicus.eu/en/products/corine-land-cover/clc2018 (accessed on 2 April 2025).
38. Tree Cover Density 2018 (TCD). Copernicus Land Monitoring Service. Available online: https://land.copernicus.eu/en/products/high-resolution-layer-forests-and-tree-cover/tree-cover-density-2018-raster-10-m-100-m-europe-yearly (accessed on 22 April 2025).
39. EEA Geospatial Data Catalogue. CORINE Land Cover 2018 (Vector). 2018. Available online: https://sdi.eea.europa.eu/catalogue/srv/api/records/53ef1493-e7a1-4216-b043-87a7c2a5a68d (accessed on 26 April 2025).
40. Pinto, M.M.; Trigo, R.M.; Trigo, I.F.; DaCamara, C.C. A Practical Method for High–Resolution Burned Area Monitoring Using Sentinel–2 and VIIRS. *Remote Sens.* **2021**, *13*, 1608. [CrossRef]
41. Lee, K.; Kim, B.; Park, S. Evaluating the potential of burn severity mapping and transferability of Copernicus EMS data using Sentinel–2 imagery and machine learning approaches. *GIScience Remote Sens.* **2023**, *60*, 2192157. [CrossRef]
42. Bruce, P.; Bruce, A.; Gedeck, P. *Practical Statistics for Data Scientists*; O'Reilly Media: Sebastopol, CA, USA, 2017; ISBN 9781492072942.
43. Faraway, J.J. *Linear Models with R*; Chapman and Hall/CRC: Riverside, CA, USA, 2004; ISBN 978-1584884255.
44. IBM Corp. *IBM SPSS Statistics for Windows, Version 30.0*; IBM Corp.: Armonk, NY, USA, 2024.

45. Sen, S.; Yildirim, I. A Tutorial on How to Conduct Meta-Analysis with IBM SPSS Statistics. *Psych* **2022**, *4*, 640–667. [CrossRef]
46. Arachchige, C.N.P.G.; Prendergast, L.A. Mean skewness measures. *arXiv* **2019**, arXiv:1912.06996. [CrossRef]
47. Veljkovic, K. Comparing Confidence Intervals for the Mean of Symmetric and Skewed Distributions. *Symmetry* **2024**, *16*, 1424. [CrossRef]
48. De Lotto, R.; Bellati, R.; Moretti, M. Correlation Methodologies between Land Use and Greenhouse Gas emissions: The Case of Pavia Province (Italy). *Air* **2024**, *2*, 86–108. [CrossRef]
49. Dillon, G.K.; Holden, Z.A.; Morgan, P.; Crimmins, M.A.; Heyerdahl, E.K.; Luce, C.H. Both topography and climate affected forest and woodland burn severity in two regions of the western US, 1984 to 2006. *Ecosphere* **2011**, *2*, 1–33. [CrossRef]
50. Holden, Z.A.; Morgan, P.; Evans, J.S. A predictive model of burn severity based on 20-year satellite-inferred burn severity data in a large southwestern US wilderness area. *For. Ecol. Manag.* **2009**, *258*, 2399–2406. [CrossRef]
51. Kane, V.R.; Cansler, C.A.; Povak, N.A.; Kane, J.T.; McGaughey, R.J.; Lutz, J.A.; Churchill, D.J.; North, M.P. Mixed severity fire effects within the Rim fire: Relative importance of local climate, fire weather, topography, and forest structure. *For. Ecol. Manag.* **2015**, *358*, 62–79. [CrossRef]
52. Cannon, J.B.; Henderson, S.K.; Bailey, M.H.; Peterson, C.J. Interactions between wind and fire disturbance in forests: Competing amplifying and buffering effects. *For. Ecol. Manag.* **2019**, *436*, 117–128. [CrossRef]
53. Mapping Copernicus EMS—Mapping. The Emergency Management Service. Available online: https://mapping.emergency.copernicus.eu/ (accessed on 10 March 2025).
54. Colson, D.; Petropoulos, G.P.; Ferentinos, K.P. Exploring the potential of Sentinels-1 & 2 of the Copernicus Mission in support of rapid and cost-effective wildfire assessment. *Int. J. Appl. Earth Obs. Geoinf.* **2018**, *73*, 262–276. [CrossRef]
55. Kovács, K.D. Evaluation of burned areas with Sentinel-2 using SNAP: The case of Kineta and Mati, Greece, July 2018. *Geogr. Tech.* **2019**, *14*, 20–38. [CrossRef]
56. Llorens, R.; Sobrino, J.A.; Fernández, C.; Fernández-Alonso, J.M.; Vega, J.A. A methodology to estimate forest fires burned areas and burn severity degrees using Sentinel-2 data. Application to the October 2017 fires in the Iberian Peninsula. *Int. J. Appl. Earth Obs. Geoinf.* **2021**, *95*, 102243. [CrossRef]
57. Colomba, L.; Farasin, A.; Monaco, S.; Greco, S.; Garza, P.; Apiletti, D.; Baralis, E.; Cerquitelli, T. A dataset for burned area delineation and severity estimation from satellite imagery. In Proceedings of the 31st ACM International Conference on Information & Knowledge Management, Atlanta, GA, USA, 17–21 October 2022; pp. 3893–3897. [CrossRef]
58. Donezar-Hoyos, U.; Albizua-Huarte, L.; Amezketa-Lizarraga, E.; Barinagarrementeria-Arrese, I.; Ciriza-Labiano, R.; de Blas-Corral, T.; Larrañaga-Urien, A.; Ros-Elso, F.; Tamés-Noriega, A.; Viñuales-Lasheras, M.; et al. The Copernicus EMS Validation service as a vector for improving the emergency mapping based on Sentinel data. *Rev. Teledetec.* **2020**, *56*, 23–34. [CrossRef]
59. Evelpidou, N.; Tzouxanioti, M.; Gavalas, T.; Spyrou, E.; Saitis, G.; Petropoulos, A.; Karkani, A. Assessment of fire effects on surface runoff erosion susceptibility: The case of the summer 2021 forest fires in Greece. *Land* **2021**, *11*, 21. [CrossRef]
60. Turco, M.; Llasat, M.C.; von Hardenberg, J.; Provenzale, A. Climate change impacts on wildfires in a Mediterranean environment. *Clim. Change* **2014**, *125*, 369–380. [CrossRef]
61. Dosiou, A.; Athinelis, I.; Katris, E.; Vassalou, M.; Kyrkos, A.; Krassakis, P.; Parcharidis, I. Employing Copernicus Land Service and Sentinel—2 Satellite Mission Data to Assess the Spatial Dynamics and Distribution of the Extreme Forest Fires of 2023 in Greece. *Fire* **2024**, *7*, 20. [CrossRef]
62. Ermitão, T.; Gouveia, C.M.; Bastos, A.; Russo, A.C. Recovery Following Recurrent Fires Across Mediterranean Ecosystems. *Glob. Change Biol.* **2024**, *30*, e70013. [CrossRef] [PubMed]
63. Saulino, L.; Rita, A.; Migliozzi, A.; Maffei, C.; Allevato, E.; Garonna, A.P.; Saracino, A. Detecting burn severity across mediterranean forest types by coupling medium–spatial resolution satellite imagery and field data. *Remote Sens.* **2020**, *12*, 741. [CrossRef]
64. Guion, A.; Turquety, S.; Polcher, J.; Pennel, R.; Bastin, S.; Arsouze, T. Droughts and heatwaves in the Western Mediterranean: Impact on vegetation and wildfires using the coupled WRF-ORCHIDEE regional model (RegIPSL). *Clim. Dyn.* **2022**, *58*, 2881–2903. [CrossRef]
65. Van, L.N.; Lee, G. Investigating the relationship between topographic variables and wildfire burn severity. *Geographies* **2025**, *5*, 47. [CrossRef]
66. Meigs, G.W.; Dunn, C.J.; Parks, S.A.; Krawchuk, M.A. Influence of topography and fuels on fire refugia probability under varying fire weather conditions in forests of the Pacific Northwest, USA. *Can. J. For. Res.* **2020**, *50*, 636–647. [CrossRef]
67. Malandra, F.; Vitali, A.; Morresi, D.; Garbarino, M.; Foster, D.E.; Stephens, S.L.; Urbinati, C. Burn severity drivers in Italian large wildfires. *Fire* **2022**, *5*, 180. [CrossRef]
68. Baker, W.L.; Hanson, C.T.; Williams, M.A.; DellaSala, D.A. Countering Omitted Evidence of Variable Historical Forests and Fire Regime in Western USA Dry Forests: The Low-Severity-Fire Model Rejected. *Fire* **2023**, *6*, 146. [CrossRef]
69. Sakulich, J.; Poulos, H.M.; Gatewood, R.G.; Wogan, K.A.; Marks, C.; Taylor, A.H. Low-Severity Wildfire Shifts Mixed Conifer Forests toward Historical Stand Structure in Guadalupe Mountains National Park, Texas, USA. *Fire* **2022**, *5*, 119. [CrossRef]

70. Lasanta, T.; Cortijos-López, M.; Errea, M.P.; Khorchani, M.; Nadal–Romero, E. An environmental management experience to control wildfires in the mid–mountain mediterranean area: Shrub clearing to generate mosaic landscapes. *Land Use Pol.* **2022**, *118*, 106147. [CrossRef]
71. Jimeno-Llorente, L.; Marcos, E.; Fernández-Guisuraga, J.M. The Effects of Fire Severity on Vegetation Structural Complexity Assessed Using SAR Data Are Modulated by Plant Community Types in Mediterranean Fire-Prone Ecosystems. *Fire* **2023**, *6*, 450. [CrossRef]